Neuronal migration depends on blood flow in the adult brain

Takashi Ogino[1,2], Akari Saito[1,2], Masato Sawada[2,3], Shoko Takemura[2], Yuzuki Hara[2], Kanami Yoshimura[2], Jiro Nagase[2], Honomi Kawase[2], Takamasa Sato[2], Hiroyuki Inada[4], Vicente Herranz-Pérez[5, 6], Yoh-suke Mukouyama[7], Masatsugu Ema[8], José Manuel García-Verdugo[5], Junichi Nabekura[4] and Kazunobu Sawamoto[2, 3*]

[1] These authors contributed equally.

[2] Department of Developmental and Regenerative Neurobiology, Nagoya City University Graduate School of Medical Sciences, Nagoya 467-8601, Japan.

[3] Division of Neural Development and Regeneration, National Institute for Physiological Sciences, Okazaki 444-8585, Japan.

[4] Division of Homeostatic Development, Department of Developmental Physiology, National Institute for Physiological Sciences, Okazaki 444-8585, Japan

[5] Laboratory of Comparative Neurobiology, Cavanilles Institute, University of Valencia, CIBERNED-ISCIII, 46980 Valencia, Spain.

[6] Department of Cell Biology, Functional Biology and Physical Anthropology, University of Valencia, 46100 Burjassot, Spain.

[7] Laboratory of Stem Cell and Neuro-Vascular Biology, Cell and Development Biology Center, National Heart, Lung, and Blood Institute, National Institutes of Health, Bethesda, MD 20892, USA.

[8] Department of Stem Cells and Human Disease Models, Research Center for Animal Life Science, Shiga University of Medical Science, Seta Tsukinowa-cho, Otsu 520-2192, Japan.

[*]Correspondence: sawamoto@med.nagoya-cu.ac.jp

Abstract

In animal tissues, several cell types migrate along blood vessels, raising the possibility that blood flow influences cell migration. Here, we show that blood flow promotes the migration of new olfactory-bulb neurons in the adult brain. Neuronal migration is facilitated by blood flow, leading to accumulation of new neurons near blood vessels with abundant blood flow. Blood flow inhibition attenuates blood vessel-guided neuronal migration, suggesting that blood contains factors beneficial to neuronal migration. We found that ghrelin, which is increased in blood by hunger, directly influences neuronal migration. Ghrelin signaling promotes somal translocation by activating actin cytoskeleton contraction at the rear of the cell soma. New neurons mature in the olfactory bulb and contribute to the olfactory function for sensing odorants from food. Finally, we show that neuronal migration is increased by calorie restriction, and that ghrelin signaling is involved in the process. This study suggests that blood flow promotes neuronal migration through blood-derived ghrelin signaling in the adult brain, which could be one of the mechanisms that improves the olfactory function for food-seeking behavior during starvation.

Introduction

Blood vessel-guided cell migration has been reported in various types of cells, including lymphatic endothelial cells in the embryonic zebrafish trunk (Bussmann et al., 2010), Schwann cells, oligodendrocyte precursor cells, glioma cells, and astrocyte progenitors in rodent tissues (Cattin et al., 2015; Farin et al., 2006; Tabata et al., 2022; Tsai et al., 2016), suggesting that it is a common mechanism for efficient cell migration within complex animal tissues. Previous reports have extensively studied the role of blood vessels as a physical scaffold for migration of neurons produced in the postnatal brain tissues (Bovetti et al., 2007; Fujioka et al., 2017; Grade et al., 2013; Ohab et al., 2006; Snapyan et al., 2009; Sun et al., 2015; Thored et al., 2007; Whitman et al., 2009; Yamashita et al., 2006). New neurons generated in the postnatal ventricular-subventricular zone (V-SVZ) migrate to the olfactory bulb (OB) through the rostral migratory stream (RMS), forming elongated aggregates called chains (Doetsch and Alvarez-Buylla, 1996; Lois et al., 1996; Lois and Alvarez-Buylla, 1994). Within the OB, new neurons migrate individually and radially and terminate their migration in the granule cell layer (GCL) or glomerular layer (GL), where they are differentiated into GABAergic interneurons and incorporated into the OB neural circuit (Bressan and Saghatelyan, 2021; Kaneko et al., 2017). Previous studies have shown that both chain-forming and individually migrating neurons use blood vessels as physical scaffolds for their migration in the RMS and OB (Bovetti et al., 2007; Snapyan et al., 2009; Whitman et al., 2009). However, whether blood flow plays a role in blood vessel-guided cell migration has not been reported.

Ghrelin, a peripheral hormone produced in the stomach, is delivered to the brain through the bloodstream and accumulates in the brain parenchyma, especially at high levels in the OB (Rhea et al., 2018). The ghrelin concentration in blood has been reported to increase during fasting (Toshinai et al., 2001; Tschöp et al., 2000). In addition to its role in regulating metabolism (Al Massadi et al., 2017; Chopin et al., 2012; Soleyman-Jahi et al., 2019; Stoyanova and Lutz, 2021), ghrelin influences neurogenesis in the V-SVZ and subgranular zone of the hippocampal dentate gyrus (Hornsby et al., 2016; Kent et al., 2015; Kim et al., 2015; Li et al., 2014, 2013; Moon et al., 2009). However, its role in blood vessel-guided neuronal migration has not been studied.

To elucidate the effects of blood flow on blood vessel-guided cell migration, we focused on neuronal migration along blood vessels in the adult RMS and OB. The results showed that new neurons migrate along blood vessels with high blood flow and that their migration is affected by changes in blood flow. We also found that ghrelin promotes neuronal migration through

activation of actin cytoskeleton contraction at the rear of the cell soma, indicating that blood flow influences neuronal migration via ghrelin signaling. Furthermore, we found that calorie restriction promotes the migration of OB neurons, suggesting that the blood flow-dependent mechanism of neuronal migration could be part of a system to improve sensory function in response to physiological change in the body.

Results

New neurons migrate along blood vessels with abundant blood flow

Previous studies have revealed that V-SVZ-derived new neurons migrate along blood vessels in the RMS and GCL (Bovetti et al., 2007; Snapyan et al., 2009; Whitman et al., 2009). However, the neuron-vessel interactions along the entire migration route remain unknown. Therefore, we first studied blood vessel-guided neuronal migration in the RMS and OB using three-dimensional imaging in 6 to 12-week-old adult mice, which enables analysis of the *in vivo* spatial relationship between new neurons and blood vessels. We measured the distance from the soma of new neurons, labeled with green fluorescent protein (GFP)-encoding adenovirus, to the nearest blood vessel labeled with RITC-Dex-GMA. The results showed that GFP+ new neurons interact closely with blood vessels in the RMS, GCL, external plexiform layer, and GL (Figure 1A–D, Supplemental Movie S1). In particular, in the RMS and GL, the majority of cells were present within 5 μm of the inner surface of vessels (Figure 1D), suggesting that new neurons in these regions frequently use blood vessels as migration scaffolds. To visualize blood vessels, we also used *Flt1-DsRed* transgenic mice, in which vascular endothelial cells were specifically labeled with DsRed (Matsumoto et al., 2012). Using *Dcx-EGFP*/*Flt1-DsRed* double transgenic mice, we observed close spatial relationships between new neurons and blood vessels (Supplemental Movies S2 and S3). Transmission electron microscopy revealed direct attachment of migratory neurons, identified as cells with an elongated cell body, a dark cytoplasm with many free ribosomes, and an electron-dense nucleus with multiple nucleoli (Doetsch et al., 1997), to thin astrocytic endfeet enwrapping blood vessels (Figure 1E), as previously reported in the RMS and GCL (Bovetti et al., 2007; Whitman et al., 2009). These results indicate that new neurons migrate along blood vessels through their entire migration route, suggesting the possibility that their movement may be influenced by blood flow.

To examine the relationship between neuronal migration and blood flow, we recorded movement of new neurons and red blood cell (RBC) flow using two-photon laser scanning microscopy. Neuronal migration was recorded in the GL of *Dcx-EGFP* mice, in which new neurons were labeled with enhanced GFP (EGFP) (Figure 1F). RBC flow was also recorded in each vessel segment in the GL by line-scan measurements (Figure 1F). We identified migrating new neurons as EGFP+ cells whose position changed during the imaging period in *Dcx-EGFP* mice, in which the majority of EGFP+ cells are stationary. Most EGFP+ migrating cells (90.2%) were located within 10 μm of the nearest vessel (Figure 1G). To compare the blood vessel-guided migration of new neurons among blood vessels with different flows, we classified the vessels into two groups, high-flow and low-flow vessels, using the median RBC flow velocity as the criterion (Figure 1H). New neurons were more abundant near high-flow vessels than near low-flow vessels (Figure 1H). These cells migrated at a small angle to the longitudinal axis of blood vessels (Figure S1), indicating that new neurons use blood vessels as migration scaffolds. Next, we compared the migration speed of new neurons between the low- and high-flow perivascular region, the area within 10 μm from the nearest vessel. Migration speed, as measured by the migration distance of the cell soma, was significantly higher in the perivascular region of high-flow vessels than in that of low-flow vessels (Figure 1I). A previous study showed that new neurons undergo discontinuous migration, including migratory and stationary periods in the GL (Liang et al., 2016). The proportion of the migratory period of new neurons in the total imaging period was larger in high-flow perivascular regions than in low-flow regions (Figure 1J). Furthermore, the maximum migration speed, calculated from two consecutive imaging frames, was significantly higher for neurons migrating along high-flow vessels than for those migrating along low-flow vessels (Figure 1K). These results suggest that neuronal migration is promoted in perivascular regions with abundant blood flow.

To compare the distribution of new neurons in perivascular regions with different blood flows in deep brain regions, we used endomucin, which has been reported to be downregulated by shear stress on vascular endothelial cells *in vitro* (Zahr et al., 2016). Endomucin-negative vessels showed higher RBC flow than endomucin-positive vessels (Figure S2A–C), indicating that endomucin can be used as a marker for RBC flow velocity *in vivo*. The density of bromodeoxyuridine (BrdU)-labeled doublecortin (Dcx)+ new neurons was higher in the perivascular region of endomucin-negative vessels than in that of endomucin-positive vessels in the GL, GCL, and RMS (Figure S2D–G), suggesting that new neurons migrate along vessels with faster blood flow throughout their migration route.

We next compared the distribution of new neurons near arteriole-side and venule-side vessels identified using SLC16A1, which is expressed in venules and venule-side capillaries (Vanlandewijck et al., 2018). The density of perivascular Dcx+/BrdU+ new neurons was significantly higher in SLC16A1-negative perivascular areas than in SLC16A1-positive areas (Figure S3A, B), indicating that they actively migrate in the vicinity of arteriole-side vessels (Figure S3C). To further examine the localization of perivascular new neurons, we analyzed the cell distribution in *NG2-DsRed* mice (Zhu et al., 2008), in which we could identify arterioles, venules, and capillaries based on the morphological differences in NG2+ mural cells as performed previously (Hartmann et al., 2015; Hill et al., 2015). Arterioles, capillaries, and venules were characterized by band-like smooth muscle cells, pericytes, and fenestrated-shaped smooth muscle cells, respectively (Figure 1L). A large proportion of Dcx+/BrdU+ new neurons was observed near capillaries in the GL (arterioles; 11.8 ± 2.39%, venules; 4.34 ± 0.212%, capillaries; 83.8 ± 2.25%) (Figure 1M). The frequency of perivascular neuronal migration was compared in arteriole-side and venule-side capillaries (defined as capillaries one to three order branches away from the nearest arterioles and venules, respectively). The density of Dcx+/BrdU+ cells was higher near arteriole-side capillaries than that near venule-side capillaries (Figure 1N). Taken together, these data suggest that most neuronal migration occurs near capillaries and that new neurons prefer capillaries on the arteriole side to those on the venule side (Figure S3C).

Because blood vessel-guided neuronal migration in the adult brain is a conserved phenomenon across species (Akter et al., 2021; Kishimoto et al., 2011; Shvedov et al., 2024), we hypothesized that blood flow may also influence neuronal migration in other brain regions of primates. The neocortex, which supports higher-order brain functions and has undergone evolutionary expansion in primates, was selected as a target region. In common marmosets, but not in mice, V-SVZ-derived new neurons migrate toward the neocortex and ventral striatum (Akter et al., 2021) (Supplemental Movies S4 and S5). In the ventral striatum of 3 to 4-month-old common marmosets, Dcx+ immature neurons localized more frequently near SLC16A1-negative vessels than near SLC16A1-positive vessels, regardless of migration modes (Figure S3D, E). A similar tendency was also observed in the neocortex (Figure S3F). These results suggest that immature neurons prefer to migrate along arteriole-side vessels in the common marmoset brain, and this phenomenon is common between rodents and primates.

Finally, we examined whether new neurons mature near high-flow vessels following their migration along these blood vessels. Neuronal maturation and blood flow were recorded in *VGAT-Venus* mice, in which GABAergic neurons are labeled with Venus. Maturation of new

neurons was confirmed by observation of the same regions with an interval of 21 days (Figure 1O). The density of newly added neurons was significantly higher near high-flow vessels than near low-flow vessels (Figure 1P). Consistently, BrdU-labeled mature neurons were frequently observed in the perivascular region of endomucin-negative vessels (Figure S2H). These results suggest that blood vessel-guided neuronal migration supplies new neurons in regions of high blood flow.

Decreases in blood flow affect neuronal migration

To investigate the effects of blood flow on neuronal migration, we performed bilateral carotid artery stenosis (BCAS), which decreases blood flow in the anterior portion of the brain (Hattori et al., 2016; Shibata et al., 2004). Lentiviruses expressing Venus were injected into the V-SVZ to label new neurons migrating toward the OB (Figure 2A). The proportion of Dcx+/Venus+ cells in the OB was significantly lower in the BCAS group compared with the Sham-operated group at 5 dpi (Figure 2B, C), suggesting that blood flow reduction impairs the tangential migration of new neurons in the RMS. To evaluate whether the reduced number of new neurons in the OB following BCAS (Figure 2B, C) is solely due to impaired migration, we examined cell proliferation and survival in the V-SVZ and RMS. Specifically, we quantified the density of Ki67+ proliferating cells and cleaved caspase-3+ apoptotic cells in the sham and BCAS groups. BCAS significantly decreased cell proliferation and increased cell death in both the V-SVZ and RMS (Figure S4), suggesting that reduced neurogenesis and/or survival may contribute to the decreased distribution of new neurons in the OB. To further examine the influence of blood flow changes on neuronal migration, we induced photothrombotic clot formation to reduce blood flow in individual vessels (Figure 2D). Migration of EGFP+ cells along vessels in *Dcx-EGFP* mice was recorded using two-photon imaging (Figure 2E). To prevent effects other than blood flow inhibition, clot formation was induced in upstream vessel fragments distant from vessels close to migrating neurons (Figure 2D). For clot formation, a restricted area of selected vessels was irradiated by a two-photon laser immediately after intravenous injection of rose bengal. Clot formation resulted in blood flow termination in downstream vessels (Figure 2F), which was followed by a decrease in the migration speed of EGFP+ new neurons along downstream vessels (Figure 2E, H). Laser irradiation without rose bengal did not affect the speed of neuronal migration (Figure 2G), indicating that the inhibition of neuronal migration was not due to laser irradiation. These data

suggest that blood flow facilitates neuronal migration in the RMS and OB and that blood contains factors influencing neuronal migration.

Ghrelin increases neuronal migration speed by promoting somal translocation

We focused on ghrelin, which can be delivered from the bloodstream to the brain parenchyma, including the OB tissue, by transcytosis across vascular walls (Rhea et al., 2018). In addition, a previous study showed that newly generated neurons expressed growth hormone secretagogue receptor 1a (GHSR1a), a ghrelin receptor, in the V-SVZ, RMS, and OB (Li et al., 2014). Consistent with this report, we detected *Ghsr1a* mRNA in Dcx+ new neurons in the VSVZ, RMS, and OB (Figure S5A). A previous study showed that migration of V-SVZ-derived new neurons is attenuated in ghrelin knockout mice (Li et al., 2014), suggesting that ghrelin stimulates neuronal migration. At first, to examine transcytosis of ghrelin in the OB, we introduced fluorescently labeled ghrelin into the bloodstream. We found accumulation of fluorescent ghrelin in the RMS and OB as reported previously (Rhea et al., 2018) (Figure 3A, B, Figure S6). Fluorescence signals were observed in vascular endothelial cells and parenchymal tissue in the RMS and OB (Figure 3B), indicating that blood-derived ghrelin crosses the vascular wall into the brain parenchyma and is delivered to new neurons. In addition, we observed high levels of fluorescent signal in vascular endothelial cells of endomucin-negative, high-flow vessels (Figure 3C, D), which suggests that transcytosis of blood-derived ghrelin may occur more frequently in these vessels, potentially due to increased endothelial endocytosis. We found that some, but not all, vessels showed particularly strong fluorescent signals in parenchymal regions adjacent to the abluminal side of vascular endothelial cells, as visualized by CD31 immunostaining (Feng et al., 2004) (Figure 3A′, A′′). To quantify this observation, we defined two regions of interest: Area I (perivascular area), within 10 μm of the abluminal surface of CD31-positive endothelium; and Area II (distant area), located 10–20 μm away (Figure 3E). Of note, Area I corresponds to the perivascular region where new neurons are frequently observed (Figure 1). To determine whether ghrelin transcytosis occurs more frequently in high-flow vessels, we quantified signal gradients in the extra-vessel regions as fold changes (Area I / Area II), as illustrated in Figure 3E. The proportion of vessel segments with >1.5-fold increases was significantly higher in endomucin-negative vessels than in endomucin-positive ones (Figure 3F). Furthermore, vessel segments with >2-fold increases were observed exclusively in the endomucin-negative group (6.48% ± 1.18%). These data suggest that, in high-flow vessels, blood-derived ghrelin accumulates more

in the immediate perivascular region than more distant areas. This supports the possibility that elevated blood flow increases the delivery of ghrelin to the vascular endothelium, enhancing its transcytosis into adjacent brain parenchyma. This mechanism may underlie the preferential migration of new neurons along high-flow perivascular regions, as shown in Figure 1.

To assess the direct effect of ghrelin on neuronal migration, we applied recombinant ghrelin to V-SVZ cultures, in which new neurons emerge and migrate as chains (Figure 4A). Ghrelin significantly increased the migration distance of these neurons (Figure 4B), indicating enhanced chain migration. We then used super-resolution time-lapse imaging to examine individually migrating neurons with or without knockdown (KD) of growth hormone secretagogue receptor 1a (GHSR1a), a ghrelin receptor expressed in V-SVZ-derived new neurons (Li et al., 2014) (Figure 4C). Ghrelin enhanced the migration speed of control cells (*lacZ*-KD) cells, indicating that it also facilitates individual migration (Figure 4D). V-SVZ-derived new neurons exhibit saltatory migration consisting of a migratory phase and a resting phase (Ota et al., 2014). Ghrelin application increased the migratory phase proportion (Figure 4E) but not the length of the migration cycle (Figure 4F), suggesting that ghrelin signaling elongates the migratory phase of neuronal migration. Cultured new neurons alternate between leading process extension and somal translocation (Figure 4C). Ghrelin application did not affect the length or speed of leading process extensions (Figure 4G, H). In contrast, the somal translocation speed and somal stride length were significantly increased by ghrelin application (Figure 4I, J). No such effects were observed in *Ghsr1a*-KD cells (Figure 4D, E, I, J), suggesting that ghrelin promotes neuronal migration through ghsr1a. Taken together, these results suggest that ghrelin signaling promotes somal translocation and thus increases the efficacy of neuronal migration.

Ghrelin signaling has been reported to regulate actin cytoskeletal dynamics in astrocytoma cells (Dixit et al., 2006), which led us to examine whether a similar mechanism operates in migrating neurons. Somal translocation of migrating cortical interneurons is driven by formation of the actin cup, an accumulation of F-actin at the rear of the cell soma (Martini and Valdeolmillos, 2010). Time-lapse imaging of cultured new neurons expressing EGFP fused to the calponin homology domain of utrophin (EGFP-UtrCH), a fluorescent reporter for F-actin (Burkel et al., 2007), revealed discontinuous formation of the actin cup at the rear of the cell soma (Figure 4K). Ghrelin application extended the duration of actin cup formation (Figure 4L) and increased the migration distance during actin cup formation (Figure 4M, Supplemental Movie S6). These effects were not observed in *Ghsr1a*-KD cells (Figure 4L, M, Supplemental Movie S7),

suggesting that GHSR1a-mediated ghrelin signaling promotes somal translocation of new neurons by activation of actin cup formation at the rear of the cell soma.

To investigate the effects of ghrelin signaling on neuronal migration in the OB *in vivo*, a mixture of lentiviruses encoding either *Ghsr1a*-KD or control shRNA was injected into the OB core of the same mouse (Figure 5A). Of the total labeled Dcx+ cells, the percentage of Dcx+ cells reaching the GL was significantly lower in the *Ghsr1a*-KD group than that in the control group (Figure 5B, C), suggesting that ghrelin enhances individual radial migration of new neurons in the OB. Coinjection of control and *Ghsr1a*-KD lentiviruses into the same site allowed us to directly compare their effects under identical conditions. However, this approach may allow reciprocal interactions between neurons infected with different constructs, potentially confounding cell-autonomous effects. To address this, we also performed separate injections of control and *Ghsr1a*-KD lentiviruses into different mice (Figure S7A). Consistent with the co-injection results, *Ghsr1a*-KD cells showed reduced distribution in the GL compared with that in control cells (Figure S7B), which supports that ghrelin signaling enhances neuronal migration in a cell-autonomous manner. When lentiviruses were injected into the V-SVZ (Figure 5D), *Ghsr1a*-KD (DsRed+) cells exhibited decreased distribution in the GL (Figure 5E, F) and increased distribution in the RMS compared with control (EmGFP+) cells (Figure 5G, H). These data indicate that ghrelin signaling facilitates both individual migration in the OB and chain migration in the RMS.

To determine whether the altered distribution of new neurons after *Ghsr1a*-KD is due to impaired migration rather than changes in cell production or survival, we assessed the effects of *Ghsr1a*-KD on the proliferation and survival of new neurons and their progenitors, which express GHSR1a (Li et al., 2014). We quantified the proportion of cleaved caspase-3+ cells and Ki67+ cells from the total labeled cells in the V-SVZ and RMS in both control and *Ghsr1a*-KD groups. We found no significant difference in cleaved caspase-3+ cell proportions between the groups (Control: 874 cells from 5 mice; *Ghsr1a*-KD: 678 cells from 7 mice), suggesting that ghrelin signaling does not influence the survival of new neurons and their progenitors. Similarly, the percentage of Ki67+ cells in the RMS was similar between the two groups (Figure S8), indicating that *Ghsr1a*-KD does not impair cell proliferation in the RMS. However, technical limitations prevented a reliable evaluation of proliferation in the V-SVZ, as lentivirus injection into this region may interfere with GHSR1a expression in not only neural progenitors and new neurons, but also other ghsr1a-expressing cell types (Zigman et al., 2006). Althogh ghrelin signaling has been reported to promote cell proliferation in the V-SVZ (Li et al., 2014), our complementary in vitro KD experiments (Figure 4C–J) and in vivo OB-core lentivirus injections (Figure 5A–C), which did not

affect the V-SVZ, consistently demonstrated that *Ghsr1a*-KD reduces neuronal migration. Taken together, our results suggest that blood-derived ghrelin enhances neuronal migration in the RMS and OB by stimulating actin cytoskeleton contraction in the cell soma, rather than by altering cell proliferation or survival.

As shown in Figure 3, ghrelin transcytosis preferentially occurs in high-flow blood vessels, indicating that ghrelin contributes to blood flow-dependent neuronal migration. However, the extent to which this process depends on ghrelin signaling remained unclear. To investigate this, we combined *Ghsr1a*-KD with BCAS. We found that BCAS reduced the percentage of *Ghsr1a*-KD new neurons reaching the OB, similar to the effect seen in control neurons (Figure S9B, see also Figure 2A–C). This suggests that blood flow influences neuronal migration even under *Ghsr1a*-KD conditions. Furthermore, we analyzed the distribution of *Ghsr1a*-KD neurons with respect to vessel flow characteristics. Even under *Ghsr1a*-KD, a higher proportion of new neurons were located in the area of endomucin-negative (high-flow) vessels compared with endomucin-positive (low-flow) vessels (Figure S9C), indicating that *Ghsr1a*-KD does not abolish the preferential association of migrating neurons with high flow vessels. These findings suggest that ghrelin signaling is involved, but is not essential, for the blood flow-dependent guidance of migrating neurons, and that additional blood-derived signals may contribute to this process.

Finally, we examined whether calorie restriction, which has been reported to increase blood ghrelin levels (Toshinai et al., 2001; Tschöp et al., 2000) , affects neuronal migration. We used a 70% calorie restriction (CR) protocol, which was previously reported to enhance hippocampal neurogenesis over 14 days (Hornsby et al., 2016). In our study, mice were fed 70% of their daily ad libitum (AL) food intake levels for 5 days (Figure 5I, Figure S10A). The proportion of labeled cells in the GL (Figure 5J) and NeuN+/Dcx- cells among BrdU+ cells in the OB (FigureS10B, C) was larger in the calorie restriction group than in the ad libitum group. However, there was no significant difference in the proportion of *Ghsr1a*-KD cells in the GL between the control and calorie restriction groups (Figure 5K). We found no significant difference in the *Ghsr1a* expression level in OB Dcx+ cells between the AL and CR groups (Figure S5B). Taken together, these data suggest that blood flow promotes the migration of OB neurons during starvation via ghrelin signaling and that promoted migration of new neurons increases the number of mature neurons in the OB.

Discussion

Previous studies have shown the role of blood vessels as physical scaffolds in the migratory routes of new neurons in various situations (Bovetti et al., 2007; Fujioka et al., 2017; Grade et al., 2013; Kojima et al., 2010; Ohab et al., 2006; Snapyan et al., 2009; Sun et al., 2015; Thored et al., 2007; Whitman et al., 2009; Yamashita et al., 2006). Proteins expressed by vascular cells have been reported to facilitate neuronal migration by binding to transmembrane receptors of new neurons (Fujioka et al., 2017; Grade et al., 2013; Ohab et al., 2006; Snapyan et al., 2009). However, whether neuronal migration is affected by blood flow remains unknown. Therefore, in this study, we focused on the specific feature of the vasculature as a pipeline for blood delivery. The effects of blood flow on neuronal migration are difficult to detect with previously used experimental procedures such as immunohistochemistry of vascular endothelial cell markers in fixed tissue sections and time-lapse live imaging of brain slice cultures. Therefore, we classified blood vessels using molecular markers that reflect blood flow properties and performed *in vivo* live imaging to record blood flow. This approach enabled us to reveal the effects of blood flow on neuronal migration.

Previous studies reported that new neurons migrate along blood vessels in the RMS and GCL of the OB (Bovetti et al., 2007; Snapyan et al., 2009; Whitman et al., 2009). In the present study, three-dimensional imaging was performed over a wide area across the entire migration route in transparent brains, where the positional relationship between new neurons and blood vessels can be observed. The results suggest that new neurons use blood vessels as migration scaffolds throughout their migration route (Figure 1A–D). The distance we found between new neurons and blood vessels was larger than that reported in a previous study (Snapyan et al., 2009). This might be due to our method of measuring the distance from the blood vessels to the cell soma of new neurons, rather than the distance to the entire new neurons. To investigate the effects of blood flow on blood vessel-guided neuronal migration, we used two-photon imaging to record neuronal migration and blood flow *in vivo* in the GL in the superficial area of the OB, which is a useful model for analyzing blood vessel-guided neuronal migration. The results suggest that new neurons migrate faster near blood vessels with high flow than in the areas of those with low flow. Neural stem cells have been reported to increase blood flow in the adult V-SVZ (Lacar et al., 2012), raising the possibility that new neurons may increase blood flow in the OB. However, our observation that inhibition of blood flow suppressed neuronal migration suggests that blood flow facilitates neuronal migration. New neurons terminated their migration and differentiated into mature interneurons in perivascular regions with abundant flow.

Thus, the blood flow-dependent mechanism of neuronal migration may supply new neurons to areas appropriate for their function.

We found that the migration speed of new neurons was decreased by blood flow reduction, suggesting that neuronal migration depends on blood flow in the adult brain. Although we cannot exclude the possibility that BCAS alters the cell proliferation or survival of new neurons, our photothrombotic clot formation experiments are better suited to directly examine how acute reductions in blood flow influence neuronal migration. These experiments allowed us to assess the migration speed of new neurons shortly after inducing localized blood flow inhibition. Based on the finding that neuronal migration was attenuated in our BCAS and photothrombosis experiments, we hypothesized that a blood-derived factor facilitates neuronal migration. A previous study demonstrated that the migration of V-SVZ-derived new neurons was attenuated in ghrelin knockout mice (Li et al., 2014). In our study, we found that the migration of cultured new neurons was enhanced by the application of ghrelin to the culture medium, and this effect was abolished by *Ghsr1a* knockdown (KD). These findings suggest that ghrelin directly stimulates neuronal migration through its receptor, GHSR1a, on new neurons. A previous study showed that GHSR1a is expressed in various regions of the brain (Zigman et al., 2006). In our experiments, new neuron-specific KD of *Ghsr1a* indicated that ghrelin signaling acts in a cell-autonomous manner to regulate neuronal migration. Nevertheless, a recent study (Stark et al., 2024) showed that GHSR1a was expressed in various cell types, including glutamatergic and GABAergic neurons, suggesting that ghrelin may also exert non-cell-autonomous effects on neuronal migration. Given the presence of diverse cell types—such as neurons, microglia, pericytes, and astrocytes—along the migratory route, it remains possible that GHSR1a activation in these neighboring cells contributes to the overall regulation of neuronal migration.

Furthermore, we identified the cellular and cytoskeletal mechanisms underlying this effect on migration. The results indicate that ghrelin enhances somal translocation during migration by activating actin cytoskeletal dynamics at the rear of the neuronal soma. We also found that ghrelin signaling increases the migration distance of cell soma, which increases the migratory phase duration. Further studies are needed to elucidate how ghrelin promotes actin cup formation in migrating neurons. Given that Rac, a Rho family GTPase, mediates actin remodeling downstream of ghrelin in astrocytoma cells (Dixit et al., 2006), it is possible that Rac may also be involved in ghrelin-induced cytoskeletal regulation in new neurons. In addition to actin remodeling, ghrelin may regulate microtubule dynamics. Ghrelin signaling was shown to modulate microtubules via SFK-dependent phosphorylation of α-tubulin (Slomiany and Slomiany, 2017),

raising the possibility that ghrelin promotes somal translocation of new neurons through coordinated regulation of both actin and microtubule networks (Kaneko et al., 2017). These results suggest that ghrelin signaling promotes neuronal migration in the RMS and OB *in vivo*, which could further strengthen our finding that blood flow plays a role in neuronal migration.

Furthermore, we found that blood-derived ghrelin crosses the vascular wall into the RMS and OB. Although we could not exclude the possibility that ghrelin is produced in the brain parenchyma (Howick et al., 2017), these results suggest that blood-derived ghrelin is provided to new neurons and promotes somal translocation by activating actin cup formation. Our results indicate that higher blood flow delivers a larger amount of ghrelin to the vascular endothelium resulting in increased ghrelin transcytosis across vascular walls. It is possible that high blood flow increases the amount of ghrelin reaching the luminal surface of vascular endothelial cells, thereby increasing the possibility of ghrelin transcytosis into the brain parenchyma. Our findings suggest that blood-derived ghrelin contributes to the blood flow-dependent neuronal migration.

Because blood ghrelin levels increase during fasting (Toshinai et al., 2001; Tschöp et al., 2000), we examined the possibility that neurogenesis in the OB is affected by feeding conditions. We found that calorie restriction promoted the migration of OB neurons, an effect which was cancelled by *Ghsr1a*-KD, suggesting that calorie restriction facilitates the OB neurogenesis through ghrelin signaling. A recent study demonstrated that fasting elevated *Ghsr1a* expression in the OB (Stark et al., 2024), raising the possibility that calorie restriction may have a similar effect. However, in our analysis, the number of *Ghsr1* mRNA puncta in Dcx+ new neurons did not differ between the AL and CR groups (Figure S5B), suggesting that calorie restriction does not alter GHSR1a expression levels in new neurons. Although we cannot exclude the possibility that calorie restriction modulates GHSR1a expression in other OB cell types, our combined calorie restriction and *Ghsr1a*-KD experiments support a cell-autonomous contribution of ghrelin signaling to calorie restriction-induced enhancement of neuronal migration. Althogh our data indicate that ghrelin signaling is essential for fasting-induced acceleration of neuronal migration, calorie restriction may also alter the concentrations of other circulating factors (Alogaiel et al., 2025; Bonnet et al., 2020; Wu et al., 2024), which could independently influence the behavior of migrating neurons. Since the supply of new neurons to the OB has been suggested to improve olfactory function in food-seeking behavior (Lazarini and Lledo, 2011), increased neurogenesis caused by long-term calorie restriction may contribute to improved olfactory function for food seeking during starvation.

The increased speed of somal translocation and elongated duration of the migratory phase in cultured new neurons are in accord with the *in vivo* increase in migration speed and duration of the migratory period of new neurons around high-flow vessels, respectively. Effective somal translocation has been suggested to be advantageous for cell migration in densely packed tissues (Kengaku, 2018). It is possible that the promotion of somal translocation by ghrelin signaling and blood flow overcomes difficulties in smooth migration of new neurons in dense tissues of the adult brain.

Our data showed that new neurons preferentially migrate along arteriole-side vessels rather than venule-side vessels in both mouse and common marmoset brains, suggesting that the mechanism of blood flow-dependent neuronal migration is conserved across rodent and primate species, as well as across brain regions. A previous study identified a ghrelin homolog in the common marmoset with high sequence similarity to the murine version (Takemi et al., 2016). In addition, the marmoset GHSR1a homolog shares 95.36 % amino acid identity with that of the mouse (https://www.ncbi.nlm.nih.gov/protein/380748978). These findings suggest that blood-derived ghrelin promotes neuronal migration in the common marmoset brain in a manner similar to that in mice. Previous reports have shown that new neurons migrate along blood vessels to damaged areas after brain injury (Fujioka et al., 2017; Grade et al., 2013; Kojima et al., 2010; Ohab et al., 2006; Thored et al., 2007; Yamashita et al., 2006). Neuronal migration may be influenced by blood flow under pathological conditions as well as during blood vessel-guided migration under the physiological conditions shown in this study. It is possible that blood contains factors in addition to ghrelin that regulate neuronal migration. Blood flow may coordinate biological events between different organs by sending beneficial factors produced outside the brain to influence regionally restricted neuronal migration. Further studies could identify unknown factors involved in the mechanism of blood flow-dependent cell migration, which could contribute to the development of blood flow-based therapies for neurological diseases.

References and Notes

Akter M, Kaneko N, Herranz-Pérez V, Nakamura S, Oishi H, García-Verdugo JM, Sawamoto K. 2021. Dynamic changes in the neurogenic potential in the ventricular-subventricular zone of common marmoset during postnatal brain development. *Cerebral Cortex* **30**:4092-4109. doi:10.1093/CERCOR/BHAA031

Al Massadi O, López M, Tschöp M, Diéguez C, Nogueiras R. 2017. Current Understanding of the Hypothalamic Ghrelin Pathways Inducing Appetite and Adiposity. *Trends Neurosci*. doi:10.1016/j.tins.2016.12.003

Alogaiel DM, Alsuwaylihi A, Alotaibi MS, Macdonald IA, Lobo DN. 2025. Effects of Ramadan intermittent fasting on hormones regulating appetite in healthy individuals: A systematic review and meta-analysis. *Clinical Nutrition* **45**:250-261. doi:10.1016/j.clnu.2025.01.005

Bonnet JP, Cardel MI, Cellini J, Hu FB, Guasch-Ferré M. 2020. Breakfast Skipping, Body Composition, and Cardiometabolic Risk: A Systematic Review and Meta-Analysis of Randomized Trials. *Obesity* **28**:1098-1109. doi:10.1002/oby.22791

Bovetti S, Hsieh YC, Bovolin P, Perroteau I, Kazunori T, Puche AC. 2007. Blood vessels form a scaffold for neuroblast migration in the adult olfactory bulb. *Journal of Neuroscience* **27**:5976-5980. doi:10.1523/JNEUROSCI.0678-07.2007

Bressan C, Saghatelyan A. 2021. Intrinsic Mechanisms Regulating Neuronal Migration in the Postnatal Brain. *Front Cell Neurosci* **14**. doi:10.3389/fncel.2020.620379

Burkel BM, Von Dassow G, Bement WM. 2007. Versatile fluorescent probes for actin filaments based on the actin-binding domain of utrophin. *Cell Motil Cytoskeleton* **64**:822-832. doi:10.1002/cm.20226

Bussmann J, Bos FL, Urasaki A, Kawakami K, Duckers HJ, Schulte-Merker S. 2010. Arteries provide essential guidance cues for lymphatic endothelial cells in the zebrafish trunk. *Development* **137**:2653-2657. doi:10.1242/dev.048207

Cattin AL, Burden JJ, Van Emmenis L, MacKenzie FE, Hoving JJA, Garcia Calavia N, Guo Y, McLaughlin M, Rosenberg LH, Quereda V, Jamecna D, Napoli I, Parrinello S, Enver T, Ruhrberg C, Lloyd AC. 2015. Macrophage-Induced Blood Vessels Guide Schwann Cell-Mediated Regeneration of Peripheral Nerves. *Cell* **162**:1127-1139. doi:10.1016/j.cell.2015.07.021

Chopin LK, Seim I, Walpole CM, Herington AC. 2012. The Ghrelin axis–does it have an appetite for cancer progression? *Endocr Rev*. doi:10.1210/er.2011-1007

Dixit VD, Weeraratna AT, Yang H, Bertak D, Cooper-Jenkins A, Riggins GJ, Eberhart CG, Taub DD. 2006. Ghrelin and the Growth Hormone Secretagogue Receptor Constitute a Novel Autocrine Pathway in Astrocytoma Motility. *Journal of Biological Chemistry* **281**:16681-16690. doi:10.1074/jbc.M600223200

Doetsch F, Alvarez-Buylla A. 1996. Network of tangential pathways for neuronal migration in adult mammalian brain. *Proceedings of the National Academy of Sciences* **93**:14895-14900. doi:10.1073/pnas.93.25.14895

Doetsch F, García-Verdugo JM, Alvarez-Buylla A. 1997. Cellular Composition and Three-Dimensional Organization of the Subventricular Germinal Zone in the Adult Mammalian Brain. *The Journal of Neuroscience* **17**:5046-5061. doi:10.1523/JNEUROSCI.17-13-05046.1997

Farin A, Suzuki SO, Weiker M, Goldman JE, Bruce JN, Canoll P. 2006. Transplanted glioma cells migrate and proliferate on host brain vasculature: A dynamic analysis. *Glia* **53**:799-808. doi:10.1002/glia.20334

Feng D, Nagy JA, Pyne K, Dvorak HF, Dvorak AM. 2004. Ultrastructural Localization of Platelet Endothelial Cell Adhesion Molecule (PECAM-1, CD31) in Vascular Endothelium. *Journal of Histochemistry & Cytochemistry* **52**:87-101. doi:10.1177/002215540405200109

Fujioka T, Kaneko N, Ajioka I, Nakaguchi K, Omata T, Ohba H, Fässler R, García-Verdugo JM, Sekiguchi K, Matsukawa N, Sawamoto K. 2017. β1 integrin signaling promotes neuronal migration along vascular scaffolds in the post-stroke brain. *EBioMedicine* **16**:195-203. doi:10.1016/j.ebiom.2017.01.005

Gong S, Zheng C, Doughty ML, Losos K, Didkovsky N, Schambra UB, Nowak NJ, Joyner A, Leblanc G, Hatten ME, Heintz N. 2003. A gene expression atlas of the central nervous system based on bacterial artificial chromosomes. *Nature* **425**:917-925. doi:10.1038/nature02033

Grade S, Weng YC, Snapyan M, Kriz J, Malva JO, Saghatelyan A. 2013. Brain-Derived Neurotrophic Factor Promotes Vasculature-Associated Migration of Neuronal Precursors toward the Ischemic Striatum. *PLoS One* **8**. doi:10.1371/journal.pone.0055039

Hartmann DA, Underly RG, Grant RI, Watson AN, Lindner V, Shih AY. 2015. Pericyte structure and distribution in the cerebral cortex revealed by high-resolution imaging of transgenic mice. *Neurophotonics* **2**:041402. doi:10.1117/1.NPh.2.4.041402

Hattori Y, Enmi JI, Iguchi S, Saito S, Yamamoto Y, Nagatsuka K, Iida H, Ihara M. 2016. Substantial Reduction of Parenchymal Cerebral Blood Flow in Mice with Bilateral Common Carotid Artery Stenosis. *Sci Rep* **6**. doi:10.1038/srep32179

Hill RA, Tong L, Yuan P, Murikinati S, Gupta S, Grutzendler J. 2015. Regional Blood Flow in the Normal and Ischemic Brain Is Controlled by Arteriolar Smooth Muscle Cell Contractility and Not by Capillary Pericytes. *Neuron* **87**:95-110. doi:10.1016/j.neuron.2015.06.001

Hornsby AKE, Redhead YT, Rees DJ, Ratcliff MSG, Reichenbach A, Wells T, Francis L, Amstalden K, Andrews ZB, Davies JS. 2016. Short-term calorie restriction enhances adult hippocampal neurogenesis and remote fear memory in a Ghsr-dependent manner. *Psychoneuroendocrinology* **63**:198-207. doi:10.1016/j.psyneuen.2015.09.023

Howick K, Griffin B, Cryan J, Schellekens H. 2017. From Belly to Brain: Targeting the Ghrelin Receptor in Appetite and Food Intake Regulation. *Int J Mol Sci* **18**:273. doi:10.3390/ijms18020273

Kanda Y. 2013. Investigation of the freely available easy-to-use software "EZR" for medical statistics. *Bone Marrow Transplant* **48**:452-458. doi:10.1038/bmt.2012.244

Kaneko N, Sawada M, Sawamoto K. 2017. Mechanisms of neuronal migration in the adult brain. *J Neurochem* **141**:835-847. doi:10.1111/jnc.14002

Kengaku M. 2018. Cytoskeletal control of nuclear migration in neurons and non-neuronal cells. *Proc Jpn Acad Ser B Phys Biol Sci*. doi:10.2183/pjab.94.022

Kent BA, Beynon AL, Hornsby AKE, Bekinschtein P, Bussey TJ, Davies JS, Saksida LM. 2015. The orexigenic hormone acyl-ghrelin increases adult hippocampal neurogenesis and enhances pattern separation. *Psychoneuroendocrinology* **51**:431-439. doi:10.1016/j.psyneuen.2014.10.015

Kim Y, Kim S, Kim C, Sato T, Kojima M, Park S. 2015. Ghrelin is required for dietary restriction-induced enhancement of hippocampal neurogenesis: lessons from ghrelin knockout mice. *Endocr J* **62**:269-275. doi:10.1507/endocrj.EJ14-0436

Kishimoto N, Alfaro-Cervello C, Shimizu K, Asakawa K, Urasaki A, Nonaka S, Kawakami K, Garcia-Verdugo JM, Sawamoto K. 2011. Migration of neuronal precursors from the telencephalic ventricular zone into the olfactory bulb in adult zebrafish. *Journal of Comparative Neurology* **519**:3549-3565. doi:10.1002/cne.22722

Kleinfeld D, Mitra PP, Helmchen F, Denk W. 1998. Fluctuations and stimulus-induced changes in blood flow observed in individual capillaries in layers 2 through 4 of rat neocortex. *Proceedings of the National Academy of Sciences* **95**:15741-15746. doi:10.1073/pnas.95.26.15741

Kojima T, Hirota Y, Ema M, Takahashi S, Miyoshi I, Okano H, Sawamoto K. 2010. Subventricular zone-derived neural progenitor cells migrate along a blood vessel scaffold toward the post-stroke striatum. *Stem Cells* **28**:545-554. doi:10.1002/stem.306

Lacar B, Herman P, Platel J-C, Kubera C, Hyder F, Bordey A. 2012. Neural Progenitor Cells Regulate Capillary Blood Flow in the Postnatal Subventricular Zone. *The Journal of Neuroscience* **32**:16435-16448. doi:10.1523/JNEUROSCI.1457-12.2012

Lazarini F, Lledo P-M. 2011. Is adult neurogenesis essential for olfaction? *Trends Neurosci* **34**:20-30. doi:10.1016/j.tins.2010.09.006

Li E, Chung H, Kim Y, Kim DH, Ryu JH, Sato T, Kojima M, Park S. 2013. Ghrelin directly stimulates adult hippocampal neurogenesis: implications for learning and memory. *Endocr J* **60**:781-789. doi:10.1507/endocrj.EJ13-0008

Li E, Kim Y, Kim S, Sato T, Kojima M, Park S. 2014. Ghrelin stimulates proliferation, migration and differentiation of neural progenitors from the subventricular zone in the adult mice. *Exp Neurol* **252**:75-84. doi:10.1016/j.expneurol.2013.11.021

Liang Y, Li K, Riecken K, Maslyukov A, Gomez-Nicola D, Kovalchuk Y, Fehse B, Garaschuk O. 2016. Long-term in vivo single-cell tracking reveals the switch of migration patterns in adult-born juxtaglomerular cells of the mouse olfactory bulb. *Cell Res* **26**:805-821. doi:10.1038/cr.2016.55

Lois C, Alvarez-Buylla A. 1994. Long-Distance Neuronal Migration in the Adult Mammalian Brain. *Science (1979)* **264**:1145-1148. doi:10.1126/science.8178174

Lois C, García-Verdugo J-M, Alvarez-Buylla A. 1996. Chain Migration of Neuronal Precursors. *Science (1979)* **271**:978-981. doi:10.1126/science.271.5251.978

Martini FJ, Valdeolmillos M. 2010. Actomyosin contraction at the cell rear drives nuclear translocation in migrating cortical interneurons. *Journal of Neuroscience* **30**:8660-8670. doi:10.1523/JNEUROSCI.1962-10.2010

Matsumoto K, Azami T, Otsu A, Takase H, Ishitobi H, Tanaka J, Miwa Y, Takahashi S, Ema M. 2012. Study of normal and pathological blood vessel morphogenesis in Flt1-tdsRed BAC Tg mice. *genesis* **50**:561-571. doi:10.1002/dvg.22031

Matsumoto M, Sawada M, García-González D, Herranz-Pérez V, Ogino T, Bang Nguyen H, Quynh Thai T, Narita K, Kumamoto N, Ugawa S, Saito Y, Takeda S, Kaneko N, Khodosevich K, Monyer H, García-Verdugo JM, Ohno N, Sawamoto K. 2019. Dynamic Changes in Ultrastructure of the Primary Cilium in Migrating Neuroblasts in the Postnatal Brain. *The Journal of Neuroscience* **39**:9967-9988. doi:10.1523/JNEUROSCI.1503-19.2019

Miyamoto T, Kuboyama K, Honda M, Ohkawa Y, Oki S, Sawamoto K. 2025. High spatial resolution gene expression profiling and characterization of neuroblasts migrating in the peri-injured cortex using photo-isolation chemistry. *Front Neurosci* **18**. doi:10.3389/fnins.2024.1504047

Miyawaki T, Morikawa S, Susaki EA, Nakashima A, Takeuchi H, Yamaguchi S, Ueda HR, Ikegaya Y. 2020. Visualization and molecular characterization of whole-brain vascular networks with capillary resolution. *Nat Commun* **11**. doi:10.1038/s41467-020-14786-z

Moon M, Kim S, Hwang L, Park S. 2009. Ghrelin regulates hippocampal neurogenesis in adult mice. *Endocr J* **56**:525-531. doi:10.1507/endocrj.K09E-089

Ohab JJ, Fleming S, Blesch A, Carmichael ST. 2006. A neurovascular niche for neurogenesis after stroke. *Journal of Neuroscience* **26**:13007-13016. doi:10.1523/JNEUROSCI.4323-06.2006

Ota H, Hikita T, Sawada M, Nishioka T, Matsumoto M, Komura M, Ohno A, Kamiya Y, Miyamoto T, Asai N, Enomoto A, Takahashi M, Kaibuchi K, Sobue K, Sawamoto K. 2014. Speed control for neuronal migration in the postnatal brain by Gmip-

mediated local inactivation of RhoA. *Nat Commun* **5**:4532. doi:10.1038/ncomms5532

Park Y-G, Sohn CH, Chen R, McCue M, Yun DH, Drummond GT, Ku T, Evans NB, Oak HC, Trieu W, Choi H, Jin X, Lilascharoen V, Wang J, Truttmann MC, Qi HW, Ploegh HL, Golub TR, Chen S-C, Frosch MP, Kulik HJ, Lim BK, Chung K. 2018. Simultaneous protection of tissue physicochemical properties using polyfunctional crosslinkers. *Nat Biotechnol*. doi:10.1038/nbt.4281

Rhea EM, Salameh TS, Gray S, Niu J, Banks WA, Tong J. 2018. Ghrelin transport across the blood-brain barrier can occur independently of the growth hormone secretagogue receptor. *Mol Metab* **18**:88-96. doi:10.1016/j.molmet.2018.09.007

Sawada M, Kaneko N, Inada H, Wake H, Kato Y, Yanagawa Y, Kobayashi K, Nemoto T, Nabekura J, Sawamoto K. 2011. Sensory input regulates spatial and subtype-specific patterns of neuronal turnover in the adult olfactory bulb. *Journal of Neuroscience* **31**:11587-11596. doi:10.1523/JNEUROSCI.0614-11.2011

Sawada M, Ohno N, Kawaguchi M, Huang S, Hikita T, Sakurai Y, Bang Nguyen H, Quynh Thai T, Ishido Y, Yoshida Y, Nakagawa H, Uemura A, Sawamoto K. 2018. PlexinD1 signaling controls morphological changes and migration termination in newborn neurons. *EMBO J* **37**. doi:10.15252/embj.201797404

Schaffer CB, Friedman B, Nishimura N, Schroeder LF, Tsai PS, Ebner FF, Lyden PD, Kleinfeld D. 2006. Two-Photon Imaging of Cortical Surface Microvessels Reveals a Robust Redistribution in Blood Flow after Vascular Occlusion. *PLoS Biol* **4**:e22. doi:10.1371/journal.pbio.0040022

Shibata M, Ohtani R, Ihara M, Tomimoto H. 2004. White matter lesions and glial activation in a novel mouse model of chronic cerebral hypoperfusion.Stroke. pp. 2598-2603. doi:10.1161/01.STR.0000143725.19053.60

Shvedov NR, Analoui S, Dafalias T, Bedell BL, Gardner TJ, Scott BB. 2024. In vivo imaging in transgenic songbirds reveals superdiffusive neuron migration in the adult brain. *Cell Rep* **43**. doi:10.1016/j.celrep.2024.113759

Slomiany BL, Slomiany A. 2017. Role of Signal-Regulated Changes in Microtubule Stability Dynamics through α-Tubulin Phosphorylation on Ser/Tyr in Modulation of Salivary Gland Matrix Metalloproteinase-9 (MMP-9) Secretion in

Response to Porphyromonas gingivalis and Ghrelin. *J Biosci Med (Irvine)* **05**:22–38. doi:10.4236/jbm.2017.52003

Snapyan M, Lemasson M, Brill MS, Blais M, Massouh M, Ninkovic J, Gravel C, Berthod F, Götz M, Barker PA, Parent A, Saghatelyan A. 2009. Vasculature guides migrating neuronal precursors in the adult mammalian forebrain via brain-derived neurotrophic factor signaling. *Journal of Neuroscience* **29**:4172–4188. doi:10.1523/JNEUROSCI.4956-08.2009

Soleyman-Jahi S, Sadeghi F, Pastaki Khoshbin A, Khani L, Roosta V, Zendehdel K. 2019. Attribution of Ghrelin to Cancer; Attempts to Unravel an Apparent Controversy. *Front Oncol*. doi:10.3389/fonc.2019.01014

Stark R, Dempsey H, Kleeman E, Sassi M, Osborne-Lawrence S, Sheybani-Deloui S, Rushby HJ, Mirth CK, Austin-Muttitt K, Mullins J, Zigman JM, Davies JS, Andrews ZB. 2024. Hunger signalling in the olfactory bulb primes exploration, food-seeking and peripheral metabolism. *Mol Metab* **89**:102025. doi:10.1016/j.molmet.2024.102025

Stoyanova I, Lutz D. 2021. Ghrelin-Mediated Regeneration and Plasticity After Nervous System Injury. *Front Cell Dev Biol*. doi:10.3389/fcell.2021.595914

Sun GJ, Zhou Y, Stadel RP, Moss J, Yong JHA, Ito S, Kawasaki NK, Phan AT, Oh JH, Modak N, Reed RR, Toni N, Song H, Ming GL. 2015. Tangential migration of neuronal precursors of glutamatergic neurons in the adult mammalian brain. *Proc Natl Acad Sci U S A* **112**:9484–9489. doi:10.1073/pnas.1508545112

Tabata H, Sasaki M, Agetsuma M, Sano H, Hirota Y, Miyajima M, Hayashi K, Honda T, Nishikawa M, Inaguma Y, Ito H, Takebayashi H, Ema M, Ikenaka K, Nabekura J, Nagata K ichi, Nakajima K. 2022. Erratic and blood vessel-guided migration of astrocyte progenitors in the cerebral cortex. *Nat Commun* **13**. doi:10.1038/s41467-022-34184-x

Takemi S, Sakata I, Apu AS, Tsukahara S, Yahashi S, Katsuura G, Iwashige F, Akune A, Inui A, Sakai T. 2016. Molecular Cloning of Ghrelin and Characteristics of Ghrelin-Producing Cells in the Gastrointestinal Tract of the Common Marmoset (Callithrix jacchus). *Zoolog Sci* **33**:497–504. doi:10.2108/zs160020

Thored P, Wood J, Arvidsson A, Cammenga J, Kokaia Z, Lindvall O. 2007. Long-term neuroblast migration along blood vessels in an area with transient angiogenesis

and increased vascularization after stroke. *Stroke* **38**:3032–3039. doi:10.1161/STROKEAHA.107.488445

Toshinai K, Mondal MS, Nakazato M, Date Y, Murakami N, Kojima M, Kangawa K, Matsukura S. 2001. Upregulation of ghrelin expression in the stomach upon fasting, insulin-induced hypoglycemia, and leptin administration. *Biochem Biophys Res Commun* **281**:1220–1225. doi:10.1006/bbrc.2001.4518

Tsai H-H, Niu J, Munji R, Davalos D, Chang J, Zhang H, Tien A-C, Kuo CJ, Chan JR, Daneman R, Fancy SPJ. 2016. Oligodendrocyte precursors migrate along vasculature in the developing nervous system. *Science (1979)* **351**:379–384. doi:10.1126/science.aad3839

Tschöp M, Smiley DL, Heiman ML. 2000. Ghrelin induces adiposity in rodents. *Nature* **407**:908–913. doi:10.1038/35038090

Vanlandewijck M, He L, Mäe MA, Andrae J, Ando K, Del Gaudio F, Nahar K, Lebouvier T, Laviña B, Gouveia L, Sun Y, Raschperger E, Räsänen M, Zarb Y, Mochizuki N, Keller A, Lendahl U, Betsholtz C. 2018. A molecular atlas of cell types and zonation in the brain vasculature. *Nature* **554**:475–480. doi:10.1038/nature25739

Wang F, Flanagan J, Su N, Wang L-C, Bui S, Nielson A, Wu X, Vo H-T, Ma X-J, Luo Y. 2012. RNAscope. *The Journal of Molecular Diagnostics* **14**:22–29. doi:10.1016/j.jmoldx.2011.08.002

Wang Y, Kakizaki T, Sakagami H, Saito K, Ebihara S, Kato M, Hirabayashi M, Saito Y, Furuya N, Yanagawa Y. 2009. Fluorescent labeling of both GABAergic and glycinergic neurons in vesicular GABA transporter (VGAT)–Venus transgenic mouse. *Neuroscience* **164**:1031–1043. doi:10.1016/j.neuroscience.2009.09.010

Whitman MC, Fan W, Rela L, Rodriguez-Gil DJ, Greer CA. 2009. Blood vessels form a migratory scaffold in the rostral migratory stream. *Journal of Comparative Neurology* **516**:94–104. doi:10.1002/cne.22093

Wu Y-K, Watson HJ, Del Re AC, Finch JE, Hardin SL, Dumain AS, Brownley KA, Baker JH. 2024. Peripheral Biomarkers of Anorexia Nervosa: A Meta-Analysis. *Nutrients* **16**:2095. doi:10.3390/nu16132095

Yamashita T, Ninomiya M, Acosta PH, García-Verdugo JM, Sunabori T, Sakaguchi M, Adachi K, Kojima T, Hirota Y, Kawase T, Araki N, Abe K, Okano H, Sawamoto K.

2006. Subventricular zone-derived neuroblasts migrate and differentiate into mature neurons in the post-stroke adult striatum. *Journal of Neuroscience* **26**:6627-6636. doi:10.1523/JNEUROSCI.0149-06.2006

Yang AC, Stevens MY, Chen MB, Lee DP, Stähli D, Gate D, Contrepois K, Chen W, Iram T, Zhang L, Vest RT, Chaney A, Lehallier B, Olsson N, du Bois H, Hsieh R, Cropper HC, Berdnik D, Li L, Wang EY, Traber GM, Bertozzi CR, Luo J, Snyder MP, Elias JE, Quake SR, James ML, Wyss-Coray T. 2020. Physiological blood-brain transport is impaired with age by a shift in transcytosis. *Nature* **583**:425-430. doi:10.1038/s41586-020-2453-z

Zahr A, Alcaide P, Yang J, Jones A, Gregory M, Dela Paz NG, Patel-Hett S, Nevers T, Koirala A, Luscinskas FW, Saint-Geniez M, Ksander B, D'Amore PA, Argüeso P. 2016. Endomucin prevents leukocyte-endothelial cell adhesion and has a critical role under resting and inflammatory conditions. *Nat Commun* **7**. doi:10.1038/ncomms10363

Zhu X, Bergles DE, Nishiyama A. 2008. NG2 cells generate both oligodendrocytes and gray matter astrocytes. *Development* **135**:145-157. doi:10.1242/dev.004895

Zigman JM, Jones JE, Lee CE, Saper CB, Elmquist JK. 2006. Expression of ghrelin receptor mRNA in the rat and the mouse brain. *J Comp Neurol* **494**:528-548. doi:10.1002/cne.20823

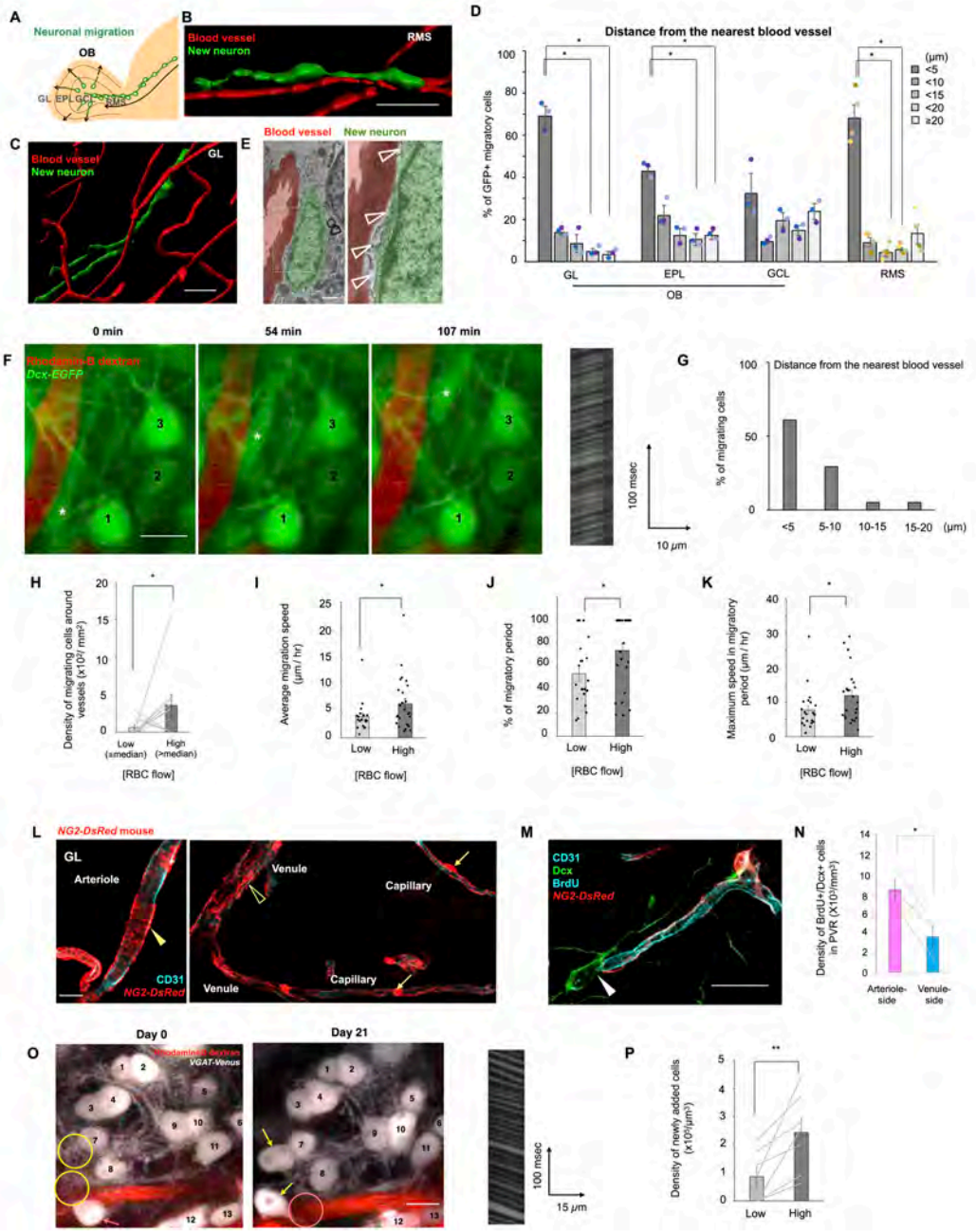

Figure 1 New neurons migrate along blood vessels with abundant flow in the adult brain.

(A) Experimental scheme.

(B, C) Three-dimensional reconstructed images of a new neuron (green) and blood vessels (red) in the rostral migratory stream (RMS) (B) and glomerular layer (GL) (C) of 6- to 12-week-old adult mice.

(D) Distance between new neurons and nearest vessels in the olfactory bulb and RMS (one-way repeated measures ANOVA followed by Bonferroni's test; 3 and 4 mice for the analysis in the OB and RMS, respectively).

(E) Transmission electron microscopy image of a new neuron (green) in close contact with a blood vessel (red) in the GL of a 6- to 12-week-old adult mouse. Astrocytes (clear arrowheads).

(F) Time-lapse images of a migrating neuron (indicated by asterisks) in the GL of a 6- to 12-week -old *Dcx-EGFP* mouse. Red blood cell (RBC) flow is recorded as a two-photon line-scan image as shown in the right panel. Stationary cells are indicated by sequential numbers.

(G) Average distance between migrating cells and nearest blood vessels (41 cells from 38 mice).

(H) Density of perivascular migrating cells (Wilcoxon signed-rank test; 10 mice).

(I) Average migration speed (Welch's *t*-test; low, 19 cells, high, 25 cells from 39 mice).

(J) Percentage of migratory period (Mann-Whitney U-test; low, 19 cells, high, 24 cells from 38 mice).

(K) Maximum migration speed (unpaired *t*-test; low, 22 cells, high, 24 cells from 39 mice).

(L) Fluorescent images in the *NG2-DsRed* mouse GL. Arterioles, capillaries, and venules were characterized by band-like smooth muscle cells (solid arrowhead), pericytes (arrows), and fenestrated smooth muscle cells (clear arrowhead), respectively. CD31 (blue), DsRed (red).

(M) Fluorescent image of a Dcx+/BrdU+ new neuron (solid arrowhead) attached to a capillary. Dcx (green), BrdU (blue), CD31 (blue, tube-like structures), DsRed (red).

(N) Density of BrdU+/Dcx+ cells in the perivascular region of arteriole-side and venule-side capillaries (paired *t*-test; 3 mice).

(O) Two-photon images of GABAergic neurons (white) and a blood vessel (red) in the *VGAT-Venus* mouse GL. Circles show positions of added (yellow) and lost (pink) Venus+ cells. Added and lost neurons are indicated by yellow and pink arrows, respectively. RBC flow on Day 21 is shown in the right panel.

(P) Density of newly added neurons in the perivascular region (paired *t*-test; 7 mice).

Data are presented as the means ± standard error of the mean (SEM). Scale bars: B, 30 μm; C, 40 μm; E, 1 μm; F, 10 μm; M, 20 μm; N, 20 μm; P, 10 μm. See also Figure. S1 and S2.

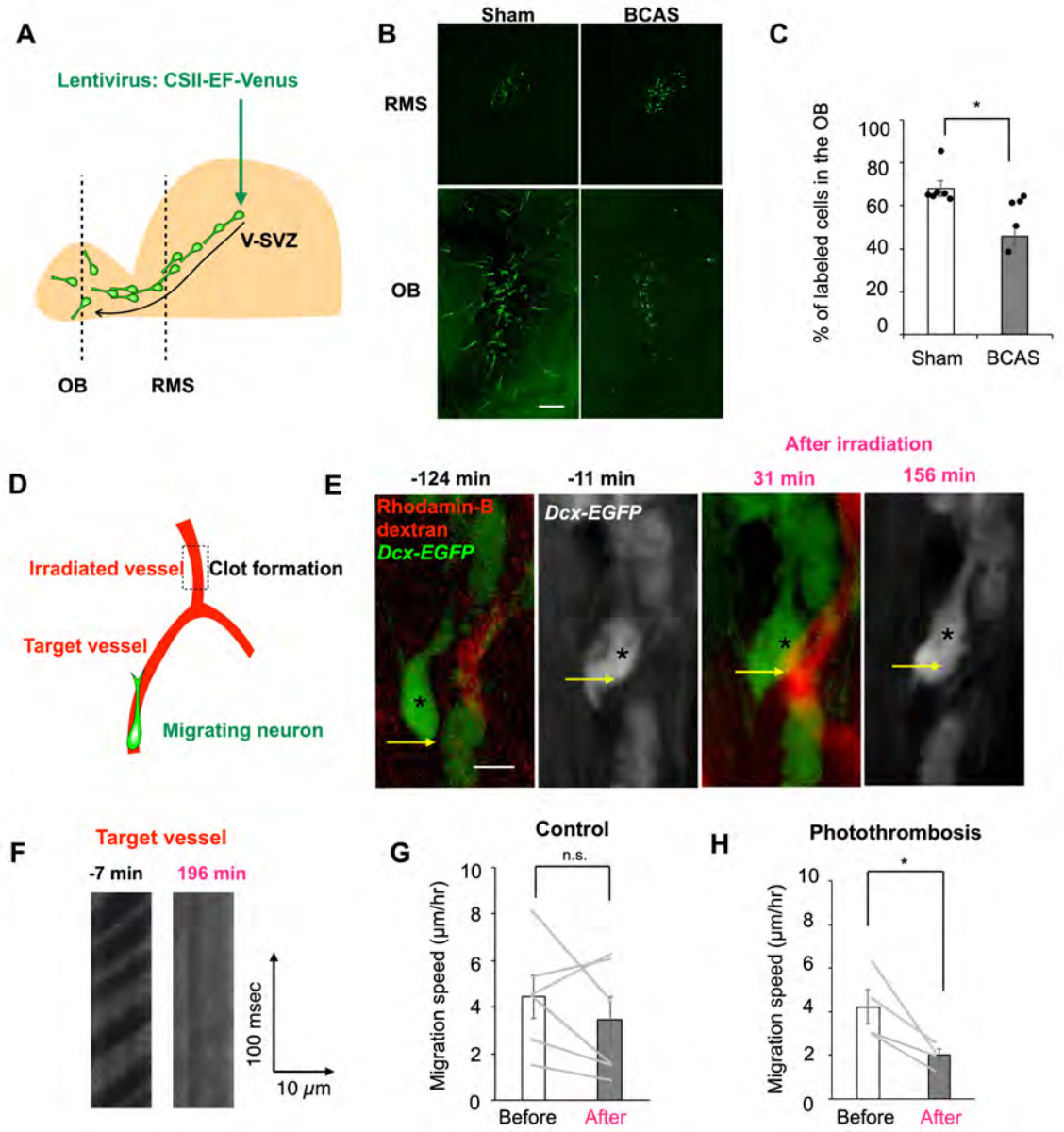

Figure 2 Blood flow inhibition attenuates neuronal migration.

(A, D) Experimental schemes.

(B) Fluorescent images of Venus+ new neurons (green) in the rostral migratory stream and olfactory bulb (OB).

(C) Proportion of Venus+ cells in the OB in the Sham and bilateral carotid artery stenosis groups (unpaired *t*-test; Sham, 6 mice, BCAS, 5 mice).

(E) Two-photon images of neuronal migration (arrows) before and after photothrombotic clot formation in a *Dcx-EGFP* mouse. A new neuron (green), a blood vessel (red).

(F) Line-scan images from a blood vessel shown in (E).

(G, H) Comparison of migration speed before and after laser irradiation in the control (G) (paired *t*-test; 7 cells from 7 mice) and photothrombosis groups (H) (paired *t*-test; 4 cells from 4 mice). Data are presented as the means ± SEM. Scale bars: B, 100 μm; E, 10 μm.

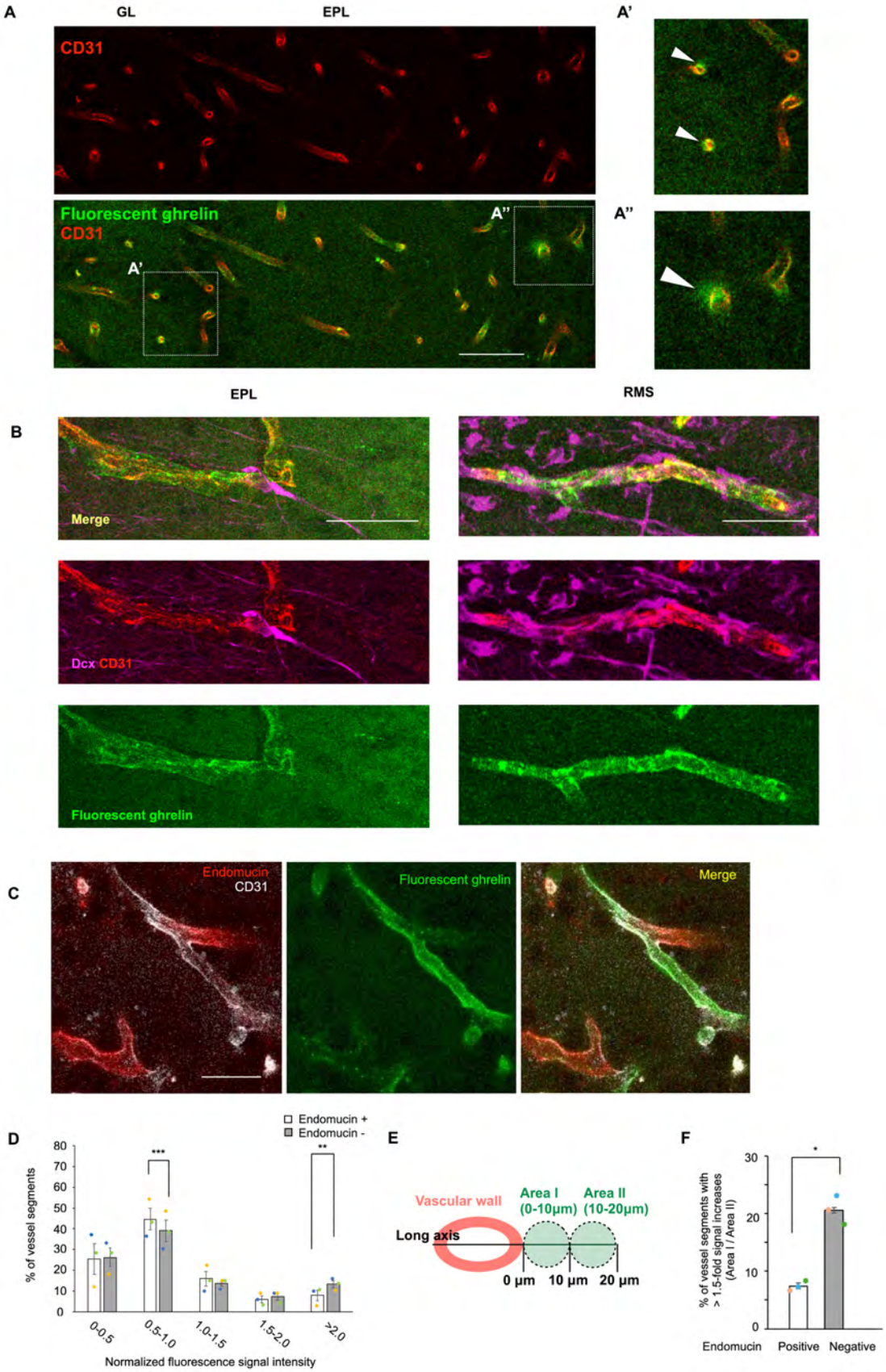
A
GL
EPL
CD31
A'
Fluorescent ghrelin
CD31
A''
A'
A''
EPL
RMS
B
Merge
Dcx CD31
Fluorescent ghrelin
C
Endomucin
CD31
Fluorescent ghrelin
Merge
D
Endomucin +
Endomucin -
% of vessel segments
Normalized fluorescence signal intensity
0-0.5
0.5-1.0
1.0-1.5
1.5-2.0
>2.0
E
Vascular wall
Area I
(0-10µm)
Area II
(10-20µm)
Long axis
0 µm
10 µm
20 µm
F
% of vessel segments with
> 1.5-fold signal increases
(Area I / Area II)
Endomucin
Positive
Negative

1

Figure 3 Ghrelin is delivered from the bloodstream to the RMS and OB in the adult brain.

(A) Representative images of the OB and the cortex of a fluorescent ghrelin-infused mouse (6- to 12-week-old). CD31 (red), Dcx (magenta), fluorescent ghrelin (green). (A′, A″) High magnification images of boxed areas in (A). Arrowheads indicate fluorescent signals in parenchymal areas adjacent to the vascular endothelium.

(B) Fluorescent images of neuronal migration along blood vessels in the EPL and the RMS. CD31 (red), Dcx (magenta), fluorescent ghrelin (green).

(C) Fluorescent images of blood vessels in the GL (C). CD31 (white), endomucin (red), fluorescent ghrelin (green).

(D) Normalized fluorescence signal intensity in vascular endothelial cells (paired *t*-test; 3 mice).

(E) Schematic diagram for analyzing signal gradients in extra-vascular areas.

(F) Percentage of vessel segments with >1.5-fold increases in Area I relative to Area II (paired *t*-test; 3 mice).

Data are presented as the means ± SEM. Scale bars: A, 50 μm; B, 20 μm (EPL), 10 μm (RMS); C, 20 μm. See also Figure. S3.

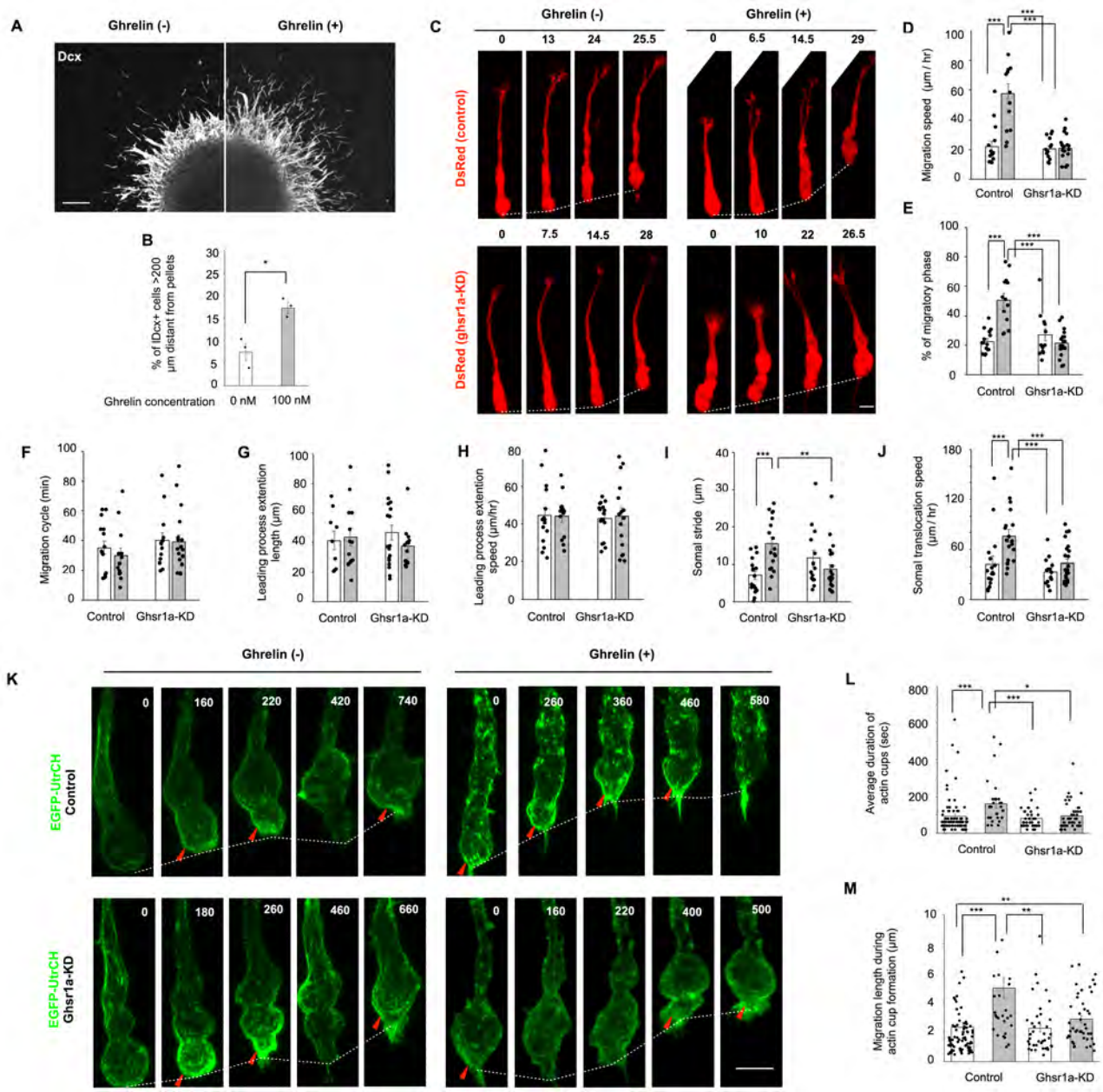

Figure 4 Ghrelin promotes neuronal migration by activation of actin cup formation.

(A) Fluorescent images of Matrigel culture. Dcx (white).

(B) Percentage of Dcx+ cells > 200 μm distant from the edge of pellets (unpaired *t*-test; 3 independent cultures prepared on different days).

(C) Time-lapse images of cultured new neurons expressing DsRed (red). The number above each panel indicates minutes after initiation of migration.

(D–J) Migration speed (D), percentage of migratory phase (E), migration cycle (F), length/speed of leading process extension (G, H), and stride/speed of somal translocation (I, J) in neuronal

migration (one-way ANOVA followed by Turkey-Kramer test; D-F; control / Ghrelin (-), 15 cells, control / Ghrelin (+), 13 cells, KD / Ghrelin (-), 13 cells, KD / Ghrelin (+), 18 cells, I, J; control / Ghrelin (-), 17 events, control / Ghrelin (+), 18 events, KD / Ghrelin (-), 14 events, KD / Ghrelin (+), 23 events).

(K) Time-lapse images of actin cup formation (arrowheads) in the cell soma of new neurons. EGFP-UtrCH (green). Condensed dots of F-actin were scattered throughout the elongated cell soma in a control cell with ghrelin application.

(L, M) Average duration of actin cups (N) and migration distance during actin cup formation (O) in new neurons (Kruskal-Wallis test followed by the Steel-Dwass test; control / Ghrelin (-), 79 cells, control / Ghrelin (+), 31 cells, KD / Ghrelin (-), 39 cells, KD / Ghrelin (+), 44 cells).

Data are presented as the means ± SEM. Scale bars: A, 100 μm; C, 5 μm; K, 5 μm.

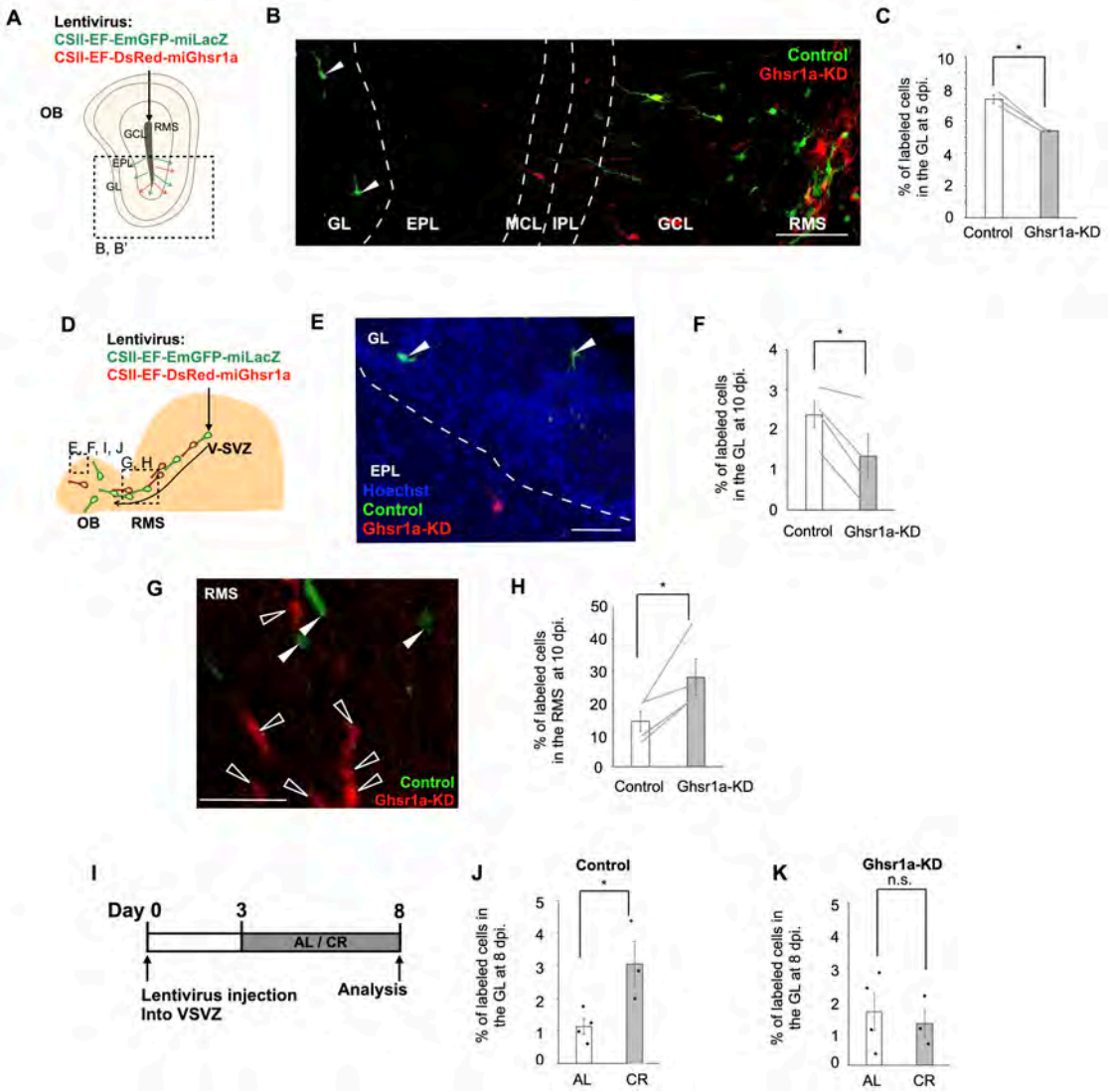

Figure 5 Ghrelin signaling promotes neuronal migration in the adult brain.

(A, D) Experimental schemes. Lentivirus injection into the OB core (A) and the VSVZ (D) was performed in 6- to 12-week-old adult mice.

(B) Fluorescent images of new neurons in the olfactory bulb in (A).

(C) Proportion of labeled cells in the GL at 5 dpi. in (A) (paired *t*-test; 3 mice).

(E, G) Fluorescent images of new neurons in the glomerular layer (GL) (E) and rostral migratory stream (RMS) (G) for the experiments shown in (D). Control cells (white arrowheads), *Ghsr1a*-KD cells (clear arrowheads).

(F, H) Proportion of labeled cells in the GL (F) and the RMS (H) at 10 dpi. in (D) (paired *t*-test; 4 mice).

(I) Experimental scheme.

(J, K) Proportion of labeled cells in the GL at 8 dpi in the ad libitum (I) and calorie restriction (J) groups (Control, unpaired *t*-test; AL, 4 mice, DR, 3 mice) (KD, unpaired *t*-test; AL, 4 mice, CR, 3 mice).

Control (green), *Ghsr1a*-KD (red). GL (glomerular layer), EPL (external plexiform layer), MCL (mitral cell layer), IPL (internal plexiform layer), GCL (granule cell layer), RMS (rostral migratory stream). AL (ad libitum), CR (calorie restriction). Data are presented as the means ± SEM. Scale bars: B, 100 μm; E, 40 μm; G, 40 μm.

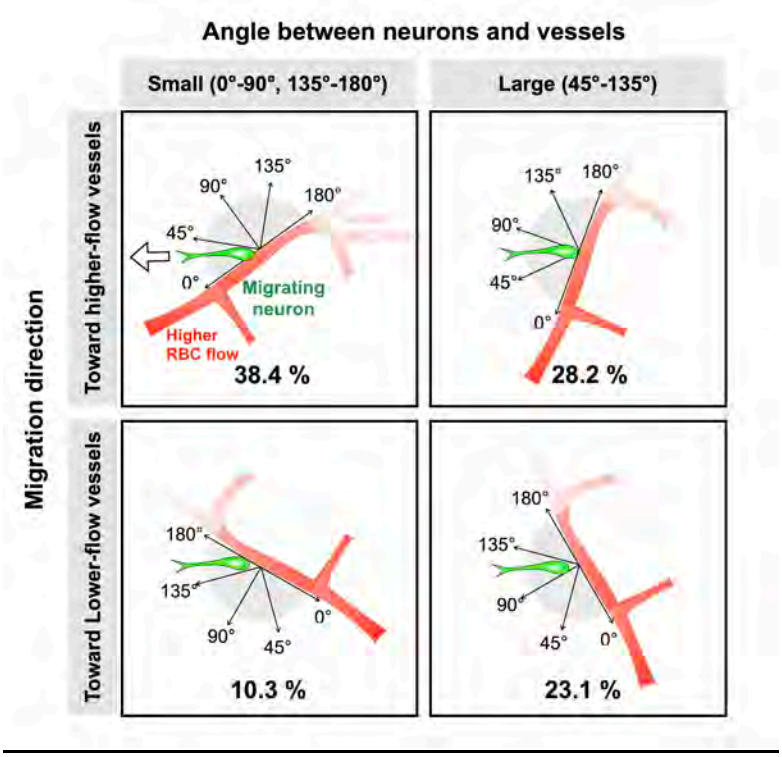

Figure S1 Directional migration of new neurons relative to local blood flow.

New neuron–vessel interactions were categorized into four groups according to the angle between the migration direction and vessel axis (small: 0°–45°, 135°–180°; large: 45°–135°), and whether the new neurons were migrating toward or away from the direction of higher red blood cell (RBC) flow. Percentages represent the proportions of total interactions (n = 39 from 26 mice).

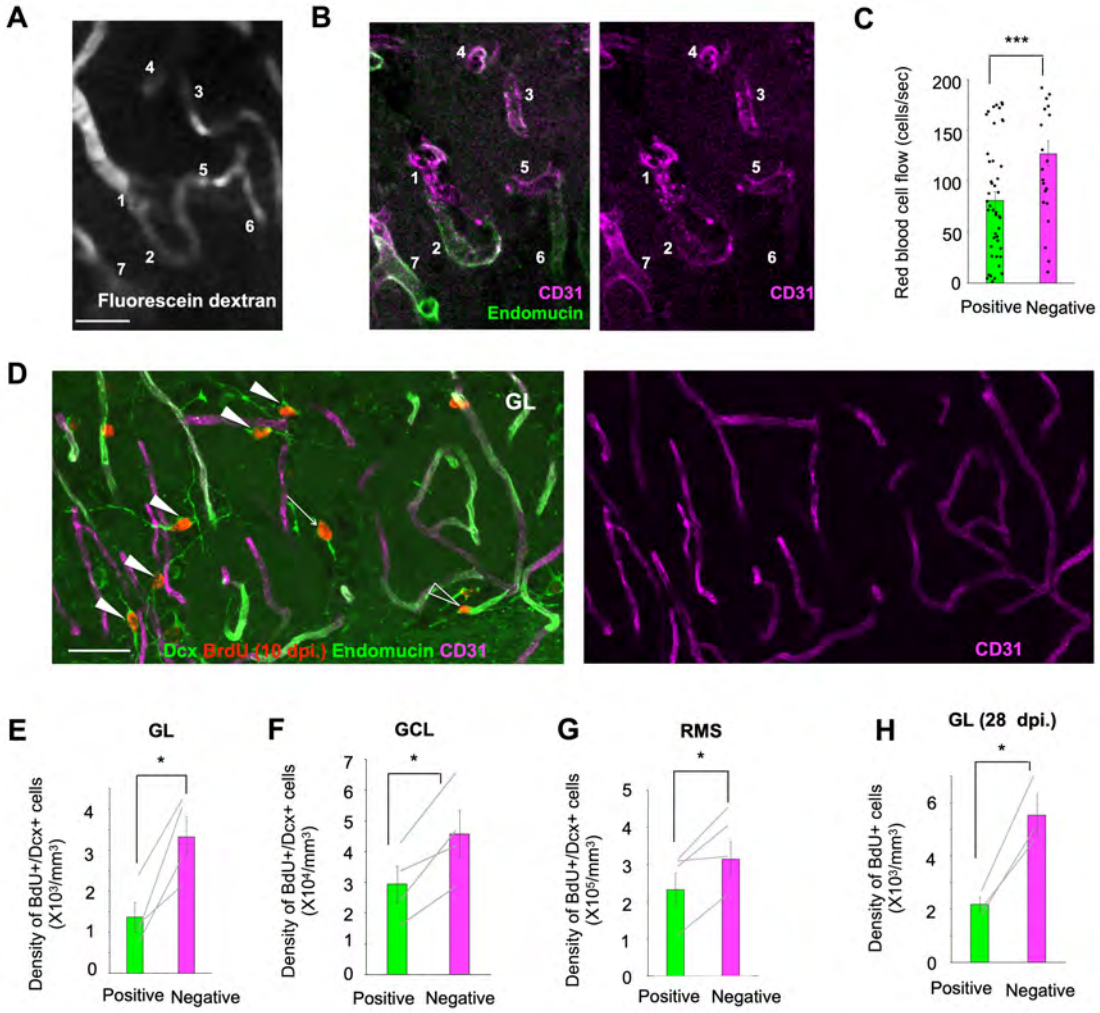

Figure S2 New neurons migrate along endomucin-negative vessels.

(A, B) Representative images of vasculature in the glomerular layer (GL) of the olfactory bulb (OB). Red blood cell (RBC) flow was recorded in a live animal (A), followed by immunostaining of endomucin/CD31 in a fixed brain section (B). Identical vessels are indicated by different numbers (endomucin-positive; 2, 6, 7, endomucin-negative; 1, 3, 4, 5).

(C) Average RBC flow in endomucin-positive and endomucin-negative vessels (Mann-Whitney U-test; endomucin-negative, 24 vessels, endomucin-positive, 46 vessels).

(D) Fluorescent image of new neurons distributed in the vasculature in the GL. BrdU+/Dcx+ cells are shown in the perivascular region of endomucin-negative vessels (white arrowheads), endomucin-positive vessels (clear arrowhead), and distant from vessels (arrow). CD31 (magenta), endomucin (green, tube-like structures), Dcx (green), BrdU (red).

(E–G) Density of BrdU+/Dcx+ cells in the vicinity of endomucin-positive and endomucin-negative vessels in the GL (E), granule cell layer (F), and rostral migratory stream (OB core) (G) (paired *t*-test; 4 mice).

(H) Density of BrdU+ mature neurons at 28 dpi. in the vicinity of endomucin-positive and endomucin-negative vessels in the GL (paired *t*-test; 4 mice).

Data are presented as the means ± SEM. Scale bars: 20 µm (A, B) ; 20 µm (D).

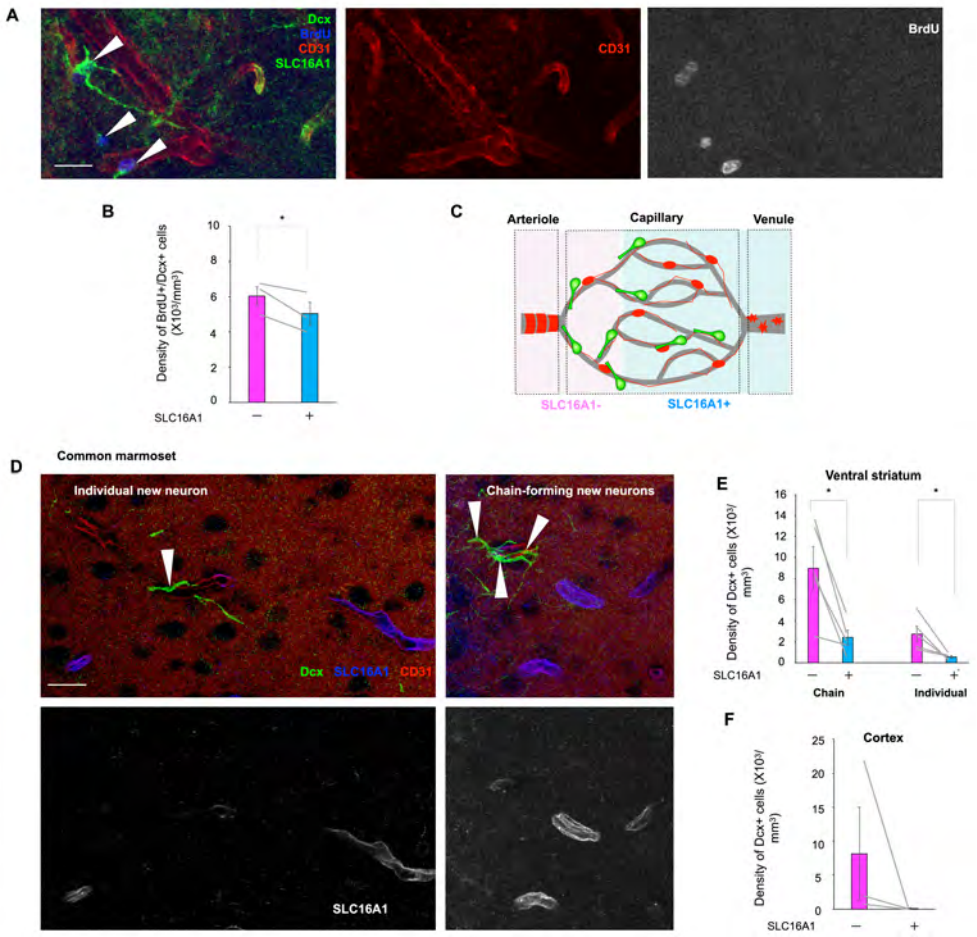

Figure S3 New neurons exhibit a preference for arteriole-side vessels.

(A) Fluorescent image of immunostained tissue sections from the glomerular layer of the olfactory bulb. Dcx (green), BrdU (deep blue), CD31 (red), SLC16A1 (green, tube-like structures).

(B) Density of perivascular new neurons in the vicinity of SLC16A1-positive and SLC16A1-negative vessels (paired *t*-test; 4 mice).

(C) Schematic illustration of the distribution of new neurons and vessel identification.

(D) Fluorescent images of the ventral striatum from a 4-month-old common marmoset. Immature neurons are indicated by solid arrowheads. Dcx (green), SLC16A1 (deep blue), CD31 (red).

(E, F) Density of BrdU+/Dcx+ cells in the vicinity of SLC16A1-positive and SLC16A1-negative vessels in the ventral striatum (E) (paired *t*-test; 5 animals) and in the neocortex (F).

Data are presented as mean ± SEM. Scale bars: 20 μm (A) ; 20 μm (D).

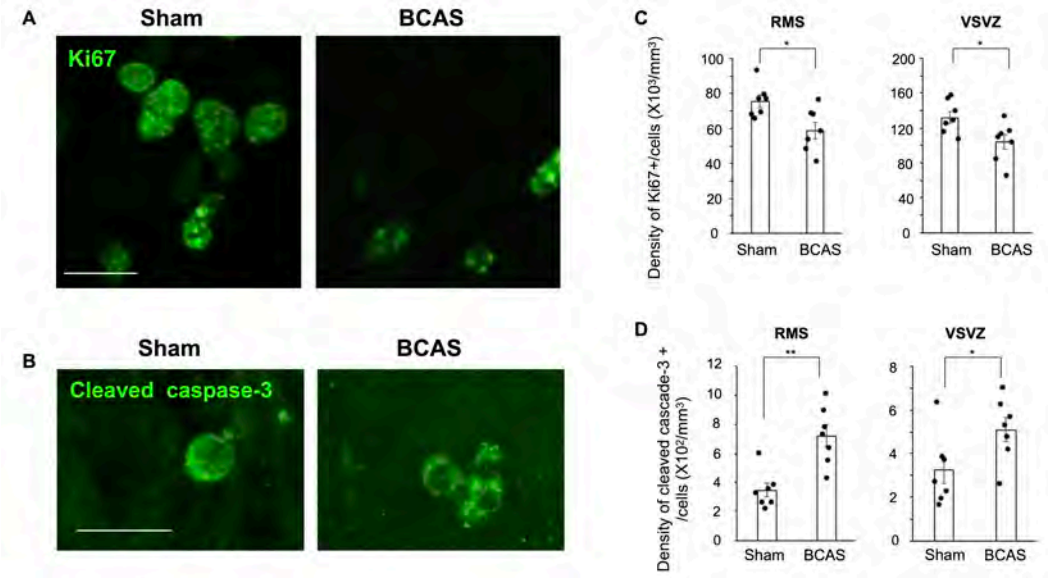

Figure S4 BCAS affects cell proliferation and survival in the VSVZ and RMS.

(A, B) Fluorescent images of immunostained RMS tissue sections showing Ki67 (green) (A) and cleaved caspase-3 (green) (B).

(C, D) Density of Ki67+ cells (C) and cleaved caspase-3+ cells (D) in the RMS and VSVZ (unpaired t-test; Sham, 7 mice, BCAS, 7 mice).

Data are presented as mean ± SEM. Scale bars: 10 μm (A, B).

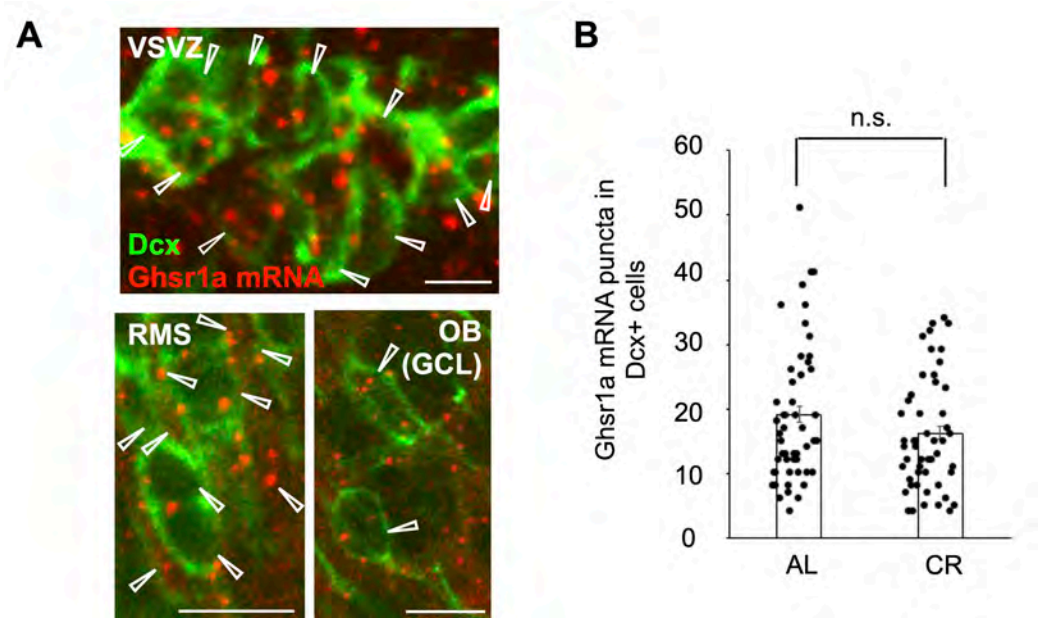

Figure S5 New neurons express *Ghsr1a* mRNA in the adult brain.

(A) Fluorescent images from the V-SVZ, RMS and OB showing Dcx (green) and *Ghsr1a* mRNA (red). Arrowheads indicate Dcx+ cells with *Ghsr1a* mRNA puncta.

(B) Quantification of *Ghsr1a* mRNA puncta per Dcx+ cell in the OB of the AL and CR mice (AL, 68 cells from 3 mice, CR, 68 cells from 3 mice).

Data are presented as mean ± SEM. Scale bars: 10 μm

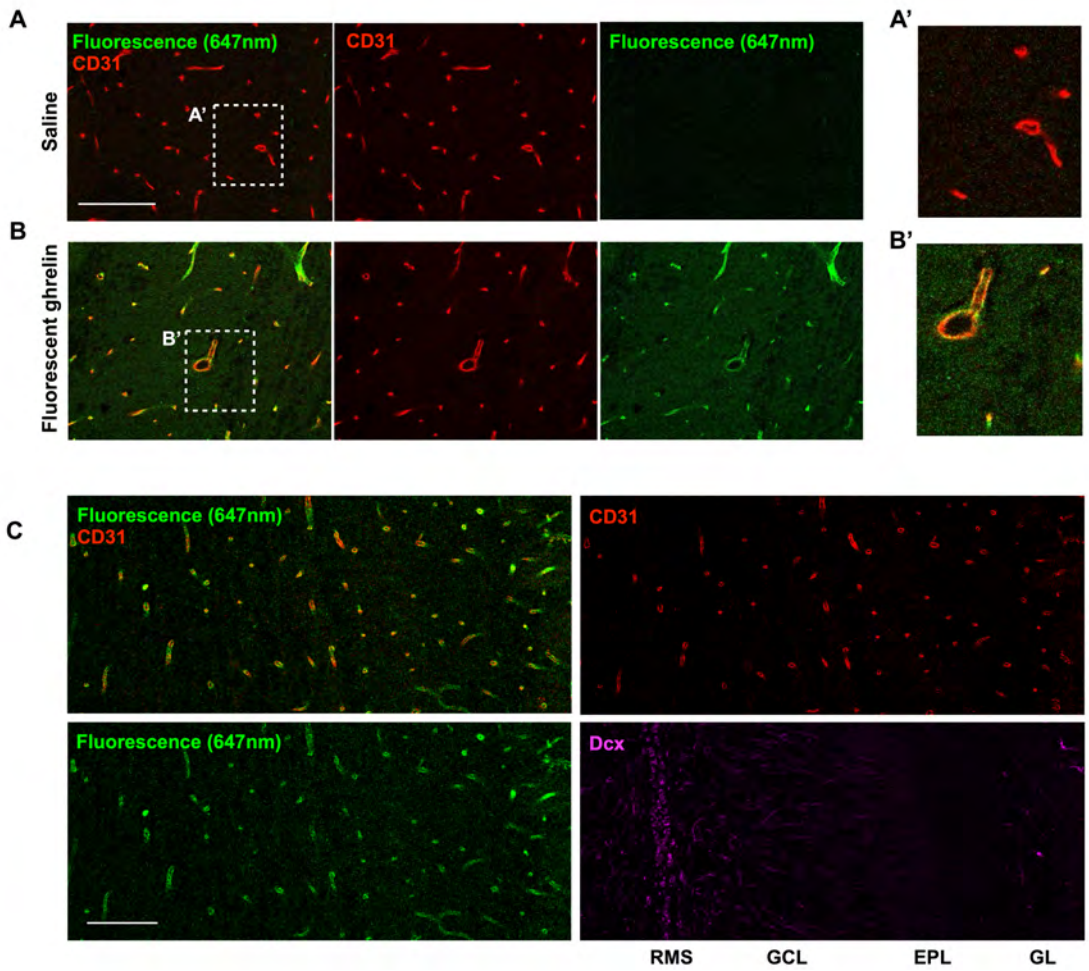

Figure S6 Blood-derived ghrelin enters the RMS and OB.

(A, B) Representative images of the OB from mice with saline injection (A) and with fluorescent ghrelin injection (B). High-magnification images are shown in (A′), (B′). It was found that the experimental process did not affect the brightness of sections. CD31 (red), fluorescence (647 nm) (green).

(C) Representative images of the OB section showing ghrelin fluorescence (647 nm, green), CD31 (red), and Dcx (magenta), covering the RMS, GCL, EPL, and GL.

Scale bars: 100 μm (A,B,C).

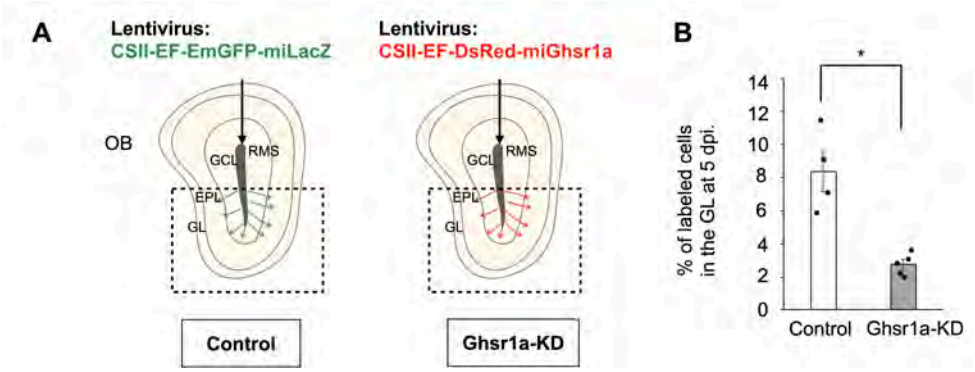

Figure S7 Ghrelin signaling is required for neuronal migration in the adult OB.

(A) Experimental schematic.

(B) Proportion of labeled cells in the GL at 5 dpi. (unpaired *t*-test; Control, 4 mice; *Ghsr1a*-KD, 5 mice).

Data are presented as mean ± SEM.

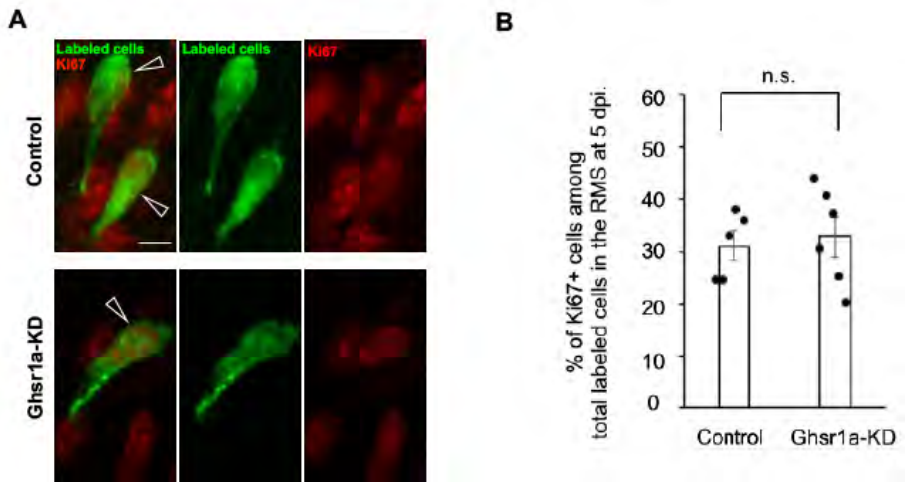

Figure S8 *Ghsr1a*-KD does not affect cell proliferation of new neurons in the RMS.

(A) Fluorescent image of immunostained RMS tissue sections showing Ki67 (red) and labeled cells (green). Ki67+ labeled cells are indicated by clear arrowheads.

(B) Quantification of Ki67+ cells as a percentage of the total labeled cells in the RMS at 5 dpi (Control, 5 mice; *Ghsr1a*-KD, 6 mice).

Data are presented as mean ± SEM. Scale bars: 5 μm (A).

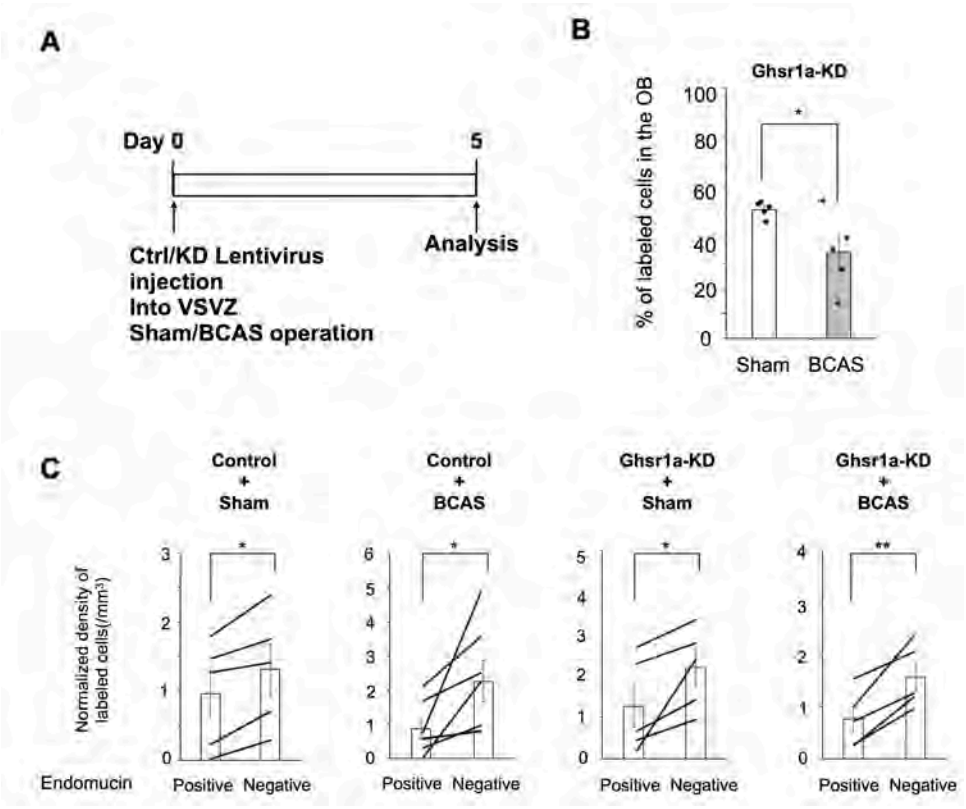

Figure S9 *Ghsr1a*-KD does not affect the influence of BCAS on neuronal migration.

(A) Experimental timeline.

(B) Proportion of *Ghsr1a*-KD cells in the OB at 5 dpi. (unpaired *t*-test; Control, 5 mice; *Ghsr1a*-KD, 5 mice).

(C) Normalized density of labeled cells in perivascular regions of the RMS (paired *t*-test; Control+Sham, 5 mice; Control+BCAS, 6 mice; *Ghsr1a*-KD+Sham, 5 mice; *Ghsr1a*-KD+BCAS, 5 mice).

Data are presented as mean ± SEM.

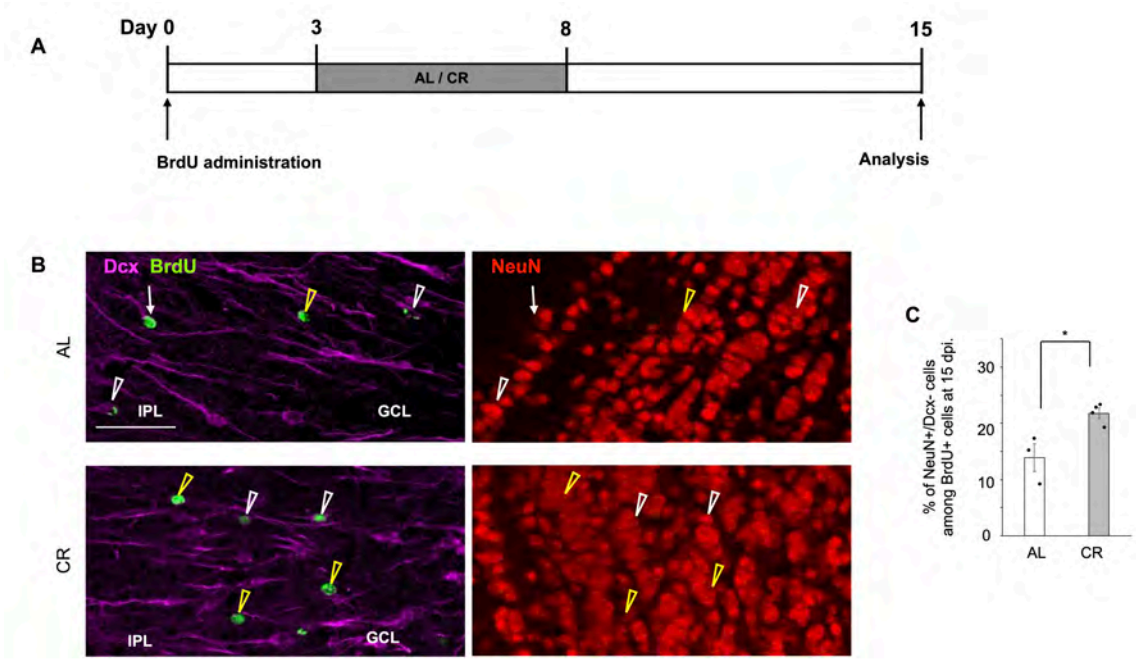

Figure S10 Calorie restriction promotes neuronal maturation in the OB.

(A) Experimental scheme.

(B) Fluorescent images of new neurons in the OB. BrdU (green), NeuN (red), Dcx (magenta). A NeuN-/Dcx+ cell (white arrow), NeuN+/Dcx+ cells (white arrowheads), NeuN+/Dcx- cells (yellow arrowheads).

(C) Proportion of NeuN+/Dcx- cells among total BrdU+ cells in the OB (KD, unpaired *t*-test; AL, 3 mice, CR, 4 mice).

IPL (internal plexiform layer), GCL (granule cell layer). Data are presented as mean ± SEM. Scale bars: 50 μm (B).

Supplemental Movie legends

Supplemental Movie S1

A three-dimensional image from the rostral migratory stream of a *Dcx-EGFP* (green) mouse infused with RITC-Dex-GMA (red).

Supplemental Movie S1′

High-magnification view extracted from Supplemental Movie S1. Arrows indicate EGFP+ cells interacting with blood vessels.

Supplemental Movie S2

A three-dimensional image from the rostral migratory stream of a *Dcx-EGFP*/*Flt1-DsRed* mouse. EGFP (green), DsRed (red).

Supplemental Movie S3

A three-dimensional, high-magnification image of chain-forming new neurons in the rostral migratory stream. *Dcx-EGFP* (green), *Flt1-DsRed* (red). Arrows indicate EGFP+ cells interacting with blood vessels.

Supplemental Movie S4

A three-dimensional image of immature neurons leaving the ventral ventricular-subventricular zone in a 1-month-old common marmoset infused with RITC-Dex-GMA (red). Dcx (green). Arrows indicate Dcx+ cells interacting with blood vessels.

Supplemental Movie S5

A three-dimensional image of an immature neuron from the ventral striatum in a 1-month-old common marmoset infused with RITC-Dex-GMA (red). Dcx (green). Arrows indicate Dcx+ cells interacting with blood vessels.

Supplemental Movie S6

Actin cup imaging in control cells. EGFP-UtrCH (green).

Supplemental Movie S7

Actin cup imaging in ghsr1a-knockdown cells. EGFP-UtrCH (green).

Methods

Animals

All *in vivo* experiments were performed on 6 to 12-week-old C57BL/6J male mice. Wild-type mice were purchased from Japan SLC (Shizuoka, Japan). The following transgenic mice were used: *Dcx-EGFP* mice (Gong et al., 2003) provided by the Mutant Mouse Research Resource Center (MMRRC), *VGAT-Venus* line #39 (Wang et al., 2009), *Flt1-DsRed* (Matsumoto et al., 2012) and *NG2-DsRed* (Zhu et al., 2008). Cells were dissociated from postnatal day 0–1 (P0–P1) pups for *in vitro* experiments. Three to four-month-old postnatal common marmosets were obtained from three mating pairs in a domestic animal colony and used for immunohistochemistry. All animals were housed under a 12-hour light /dark cycle with ad libitum access to food and water. All experiments involving live animals were performed in accordance with the guidelines and regulations of Nagoya City University and the National Institute for Physiological Sciences.

BrdU administration

Bromodeoxyuridine (BrdU, MilliporeSigma), dissolved in sterile phosphate-buffered saline (PBS), was intraperitoneally administered to mice (50 mg/kg) twice with an interval of 2 hours. Mice were fixed at 10 days post injection (dpi) to observe immature neurons or 28 dpi to observe mature olfactory neurons.

Immunohistochemistry

Immunohistochemistry was performed as previously described for brain tissues of mice (Sawada et al., 2011)and common marmosets (Akter et al., 2021). Animals were transcardially perfused with PBS (pH 7.4) followed by 4% paraformaldehyde (PFA) in 0.1 M phosphate buffer (PB). The brains were removed from the skull and postfixed in the same fixative (24 hours for mice, 48 hours for common marmosets). Coronal sections were prepared using a vibratome (VT-1200S; Leica) (50 μm thick in mice, 60 μm thick in common marmosets). The sections were incubated with 10% normal donkey serum/0.2% Triton X-100 in PBS (blocking solution) for 30 min at room temperature (RT), the primary antibodies in blocking solution for 24 hours at 4°C, and AlexaFluor-/biotin-conjugated secondary antibodies (1:1000, Invitrogen) in the same solution for 2 hours at RT. For signal amplification, the sections were pretreated with 1% H_2O_2 in PBS for 40 min at RT before blocking. The signals were amplified with biotin-conjugated antibodies and a Vectastain Elite ABC Kit (Vector Laboratories) and visualized using Tyramide Signal Amplification (Thermo Fisher Scientific). For BrdU staining, sections were treated with 1 M HCl at 37°C for 30 min after

1% H_2O_2 treatment. After staining, the sections were mounted with aqueous mounting medium (PermaFluor, Lab Vision Corporation). Z-stack images were obtained using an LSM700 confocal laser scanning microscope (Carl Zeiss) with a 20× objective (512 × 512 pixels, 1.25 μm per pixel, 1 μm z-step size). For cell density analysis, the perivascular region was defined as the area within 10 μm of the edge of CD31+ vessels. BrdU administration was performed to identify relatively immature cells in the Dcx+ cell population including newly generated cells with different differentiation states.

The following primary antibodies were used: rat anti-GFP (1:500, 04404-84, Nacalai Tesque, Inc.); rabbit anti-GFP (1:500, No. 598, Medical and Biological Laboratoies Co., LTD.); rabbit anti-DsRed (1:2000, 632496, Clontech); guinea pig anti-doublecortin (Dcx) (1:400, ab2253, MilliporeSigma); rabbit anti-Dcx (1:500, #4604, Cell Signaling Technology); rat anti-CD31 (1:100, 550274, BD Biosciences); mouse anti-human CD31 (1:100, Dako); rat anti-endomucin (1:500, sc-65495, Santa Cruz Biotechnology); rat anti-BrdU (1:100, ab6326, Abcam); rabbit anti-NeuN (1:1000, ab177487, abcam); rabbit anti-SLC16A1 (1:500, TA321556, Origene); rat anti-Ki67 (1:500, #14-5698-82, eBioscience); and rabbit anti-cleaved caspase-3 (1:200, #9661, Cell Signaling Technology). Nuclei were stained with Hoechst (1:5000, H1399, Thermo Fisher Scientific).

Three-dimensional imaging

For obtaining three-dimensional images from the rostral migratory stream (RMS), new neurons were visualized in *Dcx-EGFP* or *Dcx-EGFP/Flt1-DsRed* mice. Because the population of EGFP+ cells includes not only V-SVZ-derived migrating new neurons but also other types of cells in *Dcx-EGFP*, new neurons were labeled with adenoviruses encoding enhanced GFP (Ad-GFP, Vector Biolabs) for the analysis of new neuron-blood vessel interactions. Adenoviruses were stereotaxically injected into the V-SVZ (1.0 mm anterior, 1.1 mm lateral to bregma, and 1.6–2.0 mm deep) to label new neurons in the RMS and injected into the RMS (2.8 mm anterior, 0.82 mm lateral to bregma, and 2.8–3.0 mm deep) to label new neurons in the OB. The blood vessel lumen was visualized with RITC-Dex-GMA as previously reported with modifications (Miyawaki et al., 2020). At 5 dpi, mice were transcardially perfused with PBS and 4% PFA/0.1M PB followed by RITC-Dex-GMA. Mouse bodies were incubated in a 37°C water bath for 3 hours for polymerization. The brains were postfixed with SHIELD solutions (Lifecanvas Technologies) as previously reported (Park et al., 2018). Then, they were cleared using SmartClear II Pro (Lifecanvas Technologies). For visualization of new neurons in the common marmoset brain, the

brains were incubated in 10% normal donkey serum/ 0.5% Triton X-100 in PBS for 30 min, the anti-Dcx primary antibody in blocking solution for 5 days, and the AlexaFluor-conjugated secondary antibodies (1:1000, Invitrogen) in the same solution for 3 days at 37°C. Refractive index matching was performed using EasyIndex (Lifecanvas Technologies) before imaging. Z-stack images were acquired with a light-sheet fluorescent microscope (Carl Zeiss) with a 5× and 20× objective (1216 × 1216 pixels, 1.3 μm per pixel, 1.2–1.4 μm z-step size). Three-dimensional reconstruction was performed using Imaris software (Carl Zeiss). The three-dimensional distance was measured using ZEN software (Carl Zeiss) in light-sheet Z-stack images containing all of the GFP-positive cells in the OB hemisphere per mouse.

Bilateral carotid artery stenosis

Bilateral carotid artery stenosis was performed as previously described with modifications (Hattori et al., 2016; Shibata et al., 2004). After midline incision of the mouse cervical region, microcoils with an inner diameter of 0.18 mm (Sawane Spring Co., Ltd.) were wrapped around the common carotid arteries on both sides. Blood flow changes were confirmed by laser Doppler flowmetry in the anterior regions of brains (data not shown). A lentivirus encoding CSII-EF-Venus was stereotaxically injected into the V-SVZ to label new neurons. To analyze the cell distribution in the RMS and OB, mice were fixed at 5 dpi when glial activation is reported not to occur (Shibata et al., 2004).

Two-photon imaging

As described previously (Sawada et al., 2011), thinned-skull surgery was performed on wild-type mice for comparisons between RBC flow and endomucin expression in identical vessels and on *Dcx-EGFP* and *VGAT-Venus* mice for observation of neuronal migration and maturation, respectively. Blood vessels were visualized by intravenous injection of Rhodamine-B dextran (D1841, Invitrogen) or Fluorescein dextran (D1823, Invitrogen). Mice were anesthetized by inhalation of isoflurane. The heads were immobilized with ear bars on a stereotactic stage before surgery. The skull over the OB was carefully thinned with a high-speed drill (MINITER Co., Ltd.) and a surgical blade (Fine Science Tools). The thinned-skull window was observed under a two-photon laser scanning microscope (Nikon) and mode-locked system at 950 nm (Mai Tai HP, Spectra Physics) with a 25× water-immersion objective. Neuronal migration was recorded by identification of EGFP+ cells that changed their positions during the imaging period in the whole visible imaging field. During imaging, mice were anesthetized by intraperitoneal administration of

a mixture of medetomidine (Meiji Seika Pharma Co., Ltd.), midazolam (SANDOZ), and butorphanol (Meiji Seika Pharma Co., Ltd.) (0.75 mg/kg, 4 mg/kg, and 5 mg/kg, respectively) and kept on a heating pad for maintenance of the body temperature at 37°C. Image stacks (2048 × 2048 pixels, 0.25 μm per pixel, 2-μm z-step size) were acquired every 30–60 min during 3 hours. RBC flow was recorded by serial line-scans as previously reported (Kleinfeld et al., 1998). Line-shaped regions of interest were drawn along the longitudinal axis of each blood vessel. The RBC flow/s was calculated from repetitive scans obtained during 10 s at the beginning of the neuronal-migration recording. The median RBC flow velocity (38.4 RBCs/s) was used as a criterion for classification of vessels with different blood flows, whose distribution is not normal. Neuronal maturation was recorded as previously described with modifications (Sawada et al., 2011). After mice were anesthetized by isoflurane inhalation, the thinned-skull window was observed to record positions of Venus+ cells and RBC flow from each vessel in square-shaped regions (512 × 512 pixels, 0.5 μm per pixel, 2-μm z-step size). The same region of the GL was observed with an interval of 21 days. Stationary cells were defined as cells that were observed in the same position at both time points. Maturation and cell death in the GL were identified as addition and loss of Venus+ cells at the second time point. Data analysis was performed using NIS Element software (Nikon).

Photothrombotic clot formation

Photothrombotic clot formation was performed as previously reported with modifications (Schaffer et al., 2006). After identification of a blood vessel close to migrating neurons, an upstream vessel fragment was surrounded by a rectangular region of interest. Mice were intravenously injected with 20 mg/ml rose bengal (330000, Sigma-Aldrich) in PBS at concentration 0.05 mg/g. Immediately after injection, a selected fragment was irradiated using a two-photon laser at 950 nm. Irradiation by a 100-mW laser was performed for 5~10 seconds until the clot formed. The inner space of the vessel was equally irradiated by continuous movement of the imaging area. Ten minutes after introduction of rose bengal, the RBC flow of a target vessel was recorded to confirm blood flow inhibition. The behavior of migrating neurons was observed for 3 hours after clot formation and compared with that before photothrombosis. As a control experiment, vessels without rose Bengal injection were irradiated with a two-photon laser. Samples were excluded if bleeding occurred or clots were dissolved during observation.

Transmission electron microscopy

Transmission electron microscopy analysis was performed as previously described with modifications (Matsumoto et al., 2019; Sawada et al., 2018). Brain were fixed in 2.5% glutaraldehyde and 2% PFA in 0.1 M PB (pH 7.4) at 4°C, postfixed with 2% OsO_4 in the same buffer at 4°C, dehydrated in a graded ethanol series, placed in propyleneoxide, and embedded in Durcupan resin for 72 hours at 60°C to ensure polymerization. Ultra-thin sections (60–70 nm) were cut using an ULTRACUT-E (Reichert-Jung) with a diamond knife, stained with 2% uranyl acetate in distilled water for 15 min, and stained with modified Sato's lead solution for 5 min. Sections were analyzed with a transmission electron microscope (JEM-1011J; JEOL, Tokyo, Japan). Migratory neurons was identified as cells with an elongated cell body, a dark cytoplasm with many free ribosomes, and an electron-dense nucleus with multiple nucleoli (Doetsch et al., 1997; Matsumoto et al., 2019; Sawada et al., 2018).

Fluorescence *in situ* hybridization (RNA scope)

Fluorescence in situ hybridization was performed as previously described with modifications (Miyamoto et al., 2025) using the RNAscope multiplex assay (Advanced Cell Diagnostics), according to the manufacturer's protocol (Wang et al., 2012). After fixation with 4% PFA as described above, brains were postfixed for 4 hours at 4 °C, incubated in 15% and 30% sucrose solutions in PBS, embedded in OCT compound (Sakura Finetek Japan), and frozen using dry ice and isopentane. Serial brain sections (10 μm) were cut using a cryostat (CryoStar NX70, Epredia). The sections were fixed again in 4% PFA at RT for 30 min, dehydrated in ethanol, treated with 1% hydrogen peroxide at RT for 30 min, and then boiled in RNAscope Target Retrieval Reagent (Advanced Cell Diagnostics) at 98 °C for 15 min. Hybridization was performed using a probe targeting *Ghsr1a* mRNA (Mm-Ghsr-O2-C1, #241998, Advanced Cell Diagnostics) for 2 hours at 40 °C. Following this, immunohistochemistry with rabbit anti-Dcx antibody and Hoechst staining was conducted.

Protein labeling

For observation of ghrelin transcytosis across the vascular wall, recombinant octanoylated ghrelin (Human, sc-364689, Santa Cruz Biotechnology) was fluorescently labeled with Atto 647N NHS ester (18373, Sigma-Aldrich) as previously described with modifications (Yang et al., 2020). Ghrelin was dissolved in 0.1 M bicarbonate buffer (pH 8.3) at 2 mg/ml and reacted with Atto 647N NHS ester for 60 min at RT. After reactions, free label was removed by gel permeation chromatography with PD MiniTrap™ G-25 columns (28918007, Cytiva). Mice were fixed as

described above at 1 hour after intravenous injection of fluorescently labeled ghrelin (0.02 mg / 30g). Fluorescence signal intensity was measured by ZEN software. The average intensity among all vessels in each mouse was normalized to 1.0. To quantify signal gradients in extra-vessel regions, two circular ROIs (10 μm in diameter) were defined as illustrated in Figure 3E. The centers of the ROIs were aligned along the long axis of each vessel. Mean fluorescence intensities were measured in Area I (0–10 μm from the abluminal surface) and Area II (10–20 μm away), and fold changes (Area I / Area II) were calculated for each vessel segment.

V-SVZ culture experiments

The V-SVZ was dissected from P0–P1 mice, cut into blocks, and embedded in 60% Matrigel (BD Biosciences) in L-15 medium (Gibco). Cell aggregates were cultured in Neurobasal medium containing 2% NeuroBrew-21 (Invitrogen), 2 mM L-glutamine (Gibco), and 50 U/ml penicillin-streptomycin (Gibco) at 37°C in a 5% incubation system (Tokai Hit). For migration distance analysis, octanoylated ghrelin (Human, Rat, 1-10, Peptides International) was added to the medium at a final concentration of 100 nM at 24 hours post-embedding (hpe). Then, cell aggregates were fixed in 4% PFA/0.1M PB at 48 hpe. For immunocytochemistry, aggregates were incubated in blocking solution for 30 min at RT, treated with the primary antibodies in blocking solution for 24 hours at 4°C, and treated with AlexaFluor-secondary antibodies (1:1000) in the same solution for 2 hours at RT. The migration distance was analyzed in three independent cultures prepared on different days.

Viral vectors and plasmids

The pCSII lentiviral expression vectors were provided by Dr. Hiroyuki Miyoshi (RIKEN Tsukuba BioResource Center). The *lacZ*- and *Ghsr1a*-KD plasmids were generated as previously described (Ota et al., 2014; Sawada et al., 2018). The target sequences of *lacZ* mRNA and mouse *Ghsr1a* mRNA (Invitrogen) were inserted into modified Block-iT Poll II miR RNAi expression vectors containing EmGFP or DsRed-Express (Invitrogen). The Gateway System (Invitrogen) was used to generate pCSII-EF-Venus, pCSII-EF-Ghsr1a-IRES-Venus, pCSII-EF-EmGFP-express-miR-lacZ, pCSII-EF-DsRed-express-miR-Ghsr1a, pCAGGS-DsRed-express-miR-lacZ, and pCAGGS-DsRed-express-miR-Ghsr1a. For lentivirus production, the packaging vectors (pCAG-HIVgp, pCMV-VSV-G-RSV-Rev) and pCSII viral vectors were co-transfected into HEK-293T cells to generate lentivirus particles. Then, the culture supernatants were concentrated

by centrifugation at 8,000 rpm for 16 hours at 4°C in an MX-307 refrigerated microcentrifuge (Tomy).

***Ghsr1a* KD experiments**

The following sequence was inserted into siRNA expression vectors for targeting *Ghsr1a* mRNA: TGCTGAAGATGAGCAGATCGGAGAAGGTTTTGGCCACTGACTGACCTTCTCCGCTGCTCA TCTTCAGG. For confirming efficacy of *Ghsr1a* KD, pCSII-EF-Ghsr1a-IRES-Venus and/or pCSII-EF-DsRed-express-miR-Ghsr1a were co-transfected in HEK-293T cells. Venus signal was not observed in DsRed+ *Ghsr1a*-KD cells (data not shown).

For *in vitro* experiments, the dissected V-SVZ was dissociated with trypsin-EDTA (Invitrogen). The pCS2-EGFP-UtrCH was provided by Dr William Bement (University of Wisconsin-Madison) and Dr David J. Solecki (St. Jude Children's Research Hospital). The cells were washed in L-15 medium with 40 μg/ml DNaseI (Roche) and transfected with 2 μg plasmid DNA using the 4D-Nucleofector (Lonza). The cells were recovered in RPMI-1640 medium (Thermo Fisher Scientific) and embedded in 60% Matrigel in L-15. After cultivation in Neurobasal medium for 48 hours, time-lapse imaging was performed using an LSM880 confocal laser scanning microscope with a 40× objective (Carl Zeiss). Time-lapse images were captured at 30-s (Figure 4C–J) and 20-s (Figure 4K–M) intervals. The migration distance of cultured new neurons was measured using ImageJ manual tracking tools. A migratory phase was defined as a phase in which the cell soma traveled ≥ 30 μm during 1 hour, and a resting phase was defined as a phase in which the cell soma migrated < 30 μm. ZEN software (Carl Zeiss) was used to analyze actin cup formation. Actin cups were defined as over 4-μm-long continuous EGFP-UrtCH signals that were 1.3 times brighter than those in other cell soma regions.

For *in vivo* experiments, the lentiviral solution was stereotaxically injected into the V-SVZ and OB core of adult mice (V-SVZ: 1.0 mm anterior, 1.1 mm lateral to bregma, and 1.6–2.0 mm deep) (OB core: 4.6 mm anterior, 0.9 mm lateral to bregma, and 0.6–0.9 mm deep). The proportions of EmGFP+/DsRed- and EmGFP-/DsRed+ cells among total labeled Dcx+ new neurons in the RMS and OB were analyzed using ZEN software (Carl Zeiss). Double-positive cells (EmGFP+/DsRed+) were excluded from all analyses to avoid confounding effects of coinfection. Calorie restriction was performed as previously reported (Hornsby et al., 2016). In migration analysis, calorie-restricted animals were fed 70% of the total food consumed by animals fed ad libitum daily for the last 5 days prior to fixation at 8 dpi. In maturation analysis, calorie restriction

was performed from Day 3 to Day 8 after BrdU administration at Day 0, following fixation at Day 15.

Statistics

Statistical analysis was performed using EZR software (Kanda, 2013). The normality of the data was analyzed using a Kolmogorov-Smirnov test or Shapiro-Wilk test. The equality of variance was analyzed using an *F* test. Comparisons of data between two groups were performed with unpaired/paired *t*-tests or Welch's *t*-test for normally distributed data and by Mann-Whitney *U*-tests/Wilcoxon signed-rank tests for abnormally distributed data. Comparisons among multiple groups were performed by one-way analysis of variance (ANOVA)/one-way repeated measures ANOVA/Kruskal-Wallis tests followed by a post hoc Tukey-Kramer test, Bonferroni test, or Steel-Dwass test. Numerical data are presented as the means ± standard error of the mean. A p value < 0.05 was considered statistically significant. Significance is indicated in graphs as follows: $^{*}p < 0.05$, $^{**}p < 0.01$, $^{***}p < 0.005$, n.s., not significant.

Acknowledgements

We thank M. Agetsuma, K. Eto, T. Kobayashi, Y. Yanagawa, S. Nonaka, Y. Uchida, R. Mitsui, K. Nishimura, H. Takase, T. Fujioka, T. Miyamoto, the Laboratory Animal Facility and the Research Equipment Sharing Center at the Nagoya City University for technical support; W. Bement, D. J. Solecki, H. Miyoshi, and the MMRRC for materials; L. Kreiner and L. McCollum from Edanz and E. Nakajima for editing a draft of this manuscript, and the Sawamoto Laboratory members for helpful discussions. This work was supported by research grants from the Japan Agency for Medical Research and Development (AMED) (24gm1210007, 25ym0126807 [to K.S.]), Japan Society for the Promotion of Science (JSPS) KAKENHI (25H01040, 25H02507, 24H02016, 24K22003, 23H04939, 20H05700, 19H04757, 18KK0213, 17H05750, JP22H04926, 26640046, 22122004 [to K.S.]), Core-to-core Program "Neurogenesis Research & Innovation Center (NeuRIC)" (JPJSCCA20230007 [to KS]), Grant-in-Aid for Research at Nagoya City University (to KS), Cooperative Study Programs (22NIPS217) of the National Institute for Physiological Sciences (to K.S.), the Valencian Council for Innovation, Universities Science and Digital Society (PROMETEO/2019/075), the Spanish Ministry of Science, Innovation and Universities (PCI2018-093062), Grant-in-Aid for Promotion on Co-Creative Urban Development in Nagoya City University (2412145 [to K.S.]), Grant-in-Aid for Outstanding Research Group Support Program in

Nagoya City University Grant Number (2401101 [to K.S.]), MEXT Project for promoting public utilization of advanced research infrastructure (JPMXS0441500024), the Mizutani Foundation for Glycoscience (to K.S.), and the Takeda Science Foundation (to K.S.).

Author contributions

TO, AS, MS, ST, YH, KY, JN, HK, TS, HI, VHP, YM, ME, JMGV, JN, and KS performed experiments and analyzed the data. TO and KS wrote the manuscript.

Declaration of interests

The authors declare that they have no competing interests.

Data and materials availability

All data are available in the main text or in the supplementary materials.